Medium-strain dynamic behavior of fiber-reinforced sand subjected to stress anisotropy

Haiwen Li[1], Kostas Senetakis[2] and Matthew Coop[3]

A comprehensive database is established to investigate the behavior of polypropylene fiber reinforced sands under anisotropic stress state in a wide range of strain amplitudes from about 4×10^{-4}% to 1.4×10^{-1}%. A fixed-partly fixed Hardin-type resonant column which has a system that allows the specimen to be tested in resonance while maintaining an anisotropic loading path, is utilized. The results show important influence of the fiber content as well as the anisotropic stress state on the normalized modulus reduction and damping increase curves of the reinforced soils. Specifically, the increase of fiber content and stress ratio tend to increase the linearity in the normalized modulus reduction curves. On the other hand, the inclusion of fiber leads to the damping increase curves to shift to greater values, while the stress ratio has an opposite effect. An expression is proposed to predict the normalized shear modulus, as a function of mean effective confining pressure, stress ratio, coefficient of uniformity of the host sand and fiber content. The damping ratio, in a normalized form, is correlated with the normalized shear modulus reduction.

[1] University of New South Wales (UNSW) Sydney, Australia

[2] City University of Hong Kong, Hong Kong SAR China

[3] University College London UK

[*] (corresponding author), e-mail: ksenetak@cityu.edu.hk

1. Introduction

The application of synthetic fibers in ground improvement has been widely accepted in geotechnical engineering practice due to the increase of the shear strength (Al Refeai, 1991; Maher and Ho, 1994; Yetimoglu and Salbas, 2003; Tang et al., 2007; Diab et al., 2018; among others), and the liquefaction resistance of soils (Krishnaswamy and Isaac, 1994; Ibraim et al. 2010; Ye et al. 2017). This type of soil reinforcement can potentially apply in highway and railway embankments, retaining walls, pavements, as well as slope stability and the improvement of foundation bearing capacity (Zornberg and Kavazanjian 2002; Tutumluer et al. 2004; Park and Tan 2005; Hejazi et al. 2012).

Although the mechanics of fiber-reinforced sand has been comprehensively studied in the past few decades, especially by means of large deformation behavior, the research work on their dynamic properties remains scarce in the literature. In specific, little attention has been paid on shear modulus (G) and damping ratio of fiber reinforced soils in the range of small to medium strains under dynamic loading, within a range of strains from about 10^{-4}% to 10^{-1}%. This range of behavior is very important to be investigated and modelled with applications in geotechnical and earthquake engineering problems. For example, dynamic soil properties can be extremely nonlinear when ground motions are caused by large amplitude vibrations (such as earthquakes). As a result, the change in shear modulus and material damping ratio with shearing strain amplitude must be accounted for in ground response analysis (Lee et al., 2004; Okur and Ansal 2007; Darendeli 2001). In the range of medium strains, shear modulus reduction and damping increase curves are needed for engineering analysis and design. These values comprise properties to be used as input in variable computer programs which apply iteration processes in the study of ground shaking such as the codes SHAKE, EERA or QUAD4M (Richart et al., 1970, Kramer, 1996, Ishihara, 1996). For synthetic glass fiber – soil mixtures, Maher and Woods (1990) found that the inclusion of fibers becomes more effective at medium strain amplitudes in terms of shear modulus increase. They also noticed that the presence of fibers results in an increase of damping. Li and Senetakis (2017) found that the small-strain shear modulus of a silica crushed rock reinforced with polypropylene fibers decreased with the increase of fiber content, which observation is in agreement with the study by Clariá and Vettorelo (2015). They attributed this behavior, predominantly, to the possible negative contribution of the fibers in transferring the normal contact forces through the solid skeleton. Prior to these studies, Heineck et al. (2005) reported a negligible effect of fiber inclusion on the small-strain shear modulus of different types of soils, but it is acknowledged that the study by Heineck et al. focused on fiber percentages up to 0.5%. In the range of medium-strain amplitudes, Li and Senetakis (2018a) demonstrated that a well-graded crushed rock with irregularly shaped grains reinforced with polypropylene fibers exhibited greater linearity of the normalized modulus reduction curves in comparison to the unreinforced sand at medium strain levels.

The dynamic behavior of fiber-reinforced soils under isotropic loading has only been examined in a limited number of research works (e.g. Maher and Woods, 1990; Li and Senetakis, 2017; Li et al., 2017). However, soils in earth structures, including soils beneath foundations or natural soils under K_0 condition or slopes, are invariably subjected to anisotropic stress state (Bellotti et al., 1996; Zdravkovic and Jardine 1997; Kuwano et al., 2000). Payan et al. (2016), Chen et al. (2016) and Li and

Senetakis (2018b) have demonstrated this important effect on the dynamic properties of sands at small and small-to-medium strain amplitudes, respectively. A few research works have illustrated the effect of fiber on the dynamic properties of fiber-soil mixture under anisotropic stress condition. Senetakis and Li (2017) reported that the inclusion of fibers tends to increase the sensitivity of the normalized small-strain shear modulus to the stress anisotropy. In that study, the normalized small-strain shear modulus was expressed as the ratio of the small-strain modulus under an anisotropic stress state over the corresponding modulus under an isotropic stress stage, at a given mean effective confining pressure (p'). Similarly, Li *et al*. (2017) studied the behavior of uniform recycled concrete aggregate reinforced with carbon fibers subjected to p' constant triaxial compression stress path. They found that the addition of fibers has positive effect on the increase rate of stiffness under an anisotropic stress state in comparison to the isotropic stress state.

Even though laboratory experiments and practice indicate important contribution of fibers in the reinforcement of soils subjected to static or dynamic loading (Maher and Gray, 1990; Michalowski and Cermák, 2003; Ibraim et al., 2012; Li et al., 2017; Madhusudhan et al., 2017; Ye et al., 2017), to the authors' best knowledge, there is relatively limited information in the literature on the medium-strain behavior of fiber-reinforced soils, especially applying stress anisotropy. Therefore, the motivation behind this work was to fill this literature gap and provide a comprehensive database of experimental results covering a wide range of sand types reinforced with polypropylene fibers, which type of fibers has been examined extensively in the literature particularly in terms of reinforcing component against static behavior of soils. Based on this new database, an expression of normalized shear modulus reduction for fiber reinforced sands is developed taking into account the effect of grain size characteristics of the host sand, the content of fiber, the mean effective confining pressure and the stress ratio. Additionally, a direct correlation between damping increase and normalized modulus reduction was implemented. The proposed expressions for normalized shear modulus reduction and damping increase curves are then verified independently using a separate set of experimental data.

2. Materials and Methods

2.1 Materials of major testing program

The experiments were conducted on different fractions of a well-graded crushed rock, named as Blue sand 1 with origin from Sydney, which soil can be considered a typical fill-backfill material. Three different samples, which are derived from Blue sand 1, with different coefficients of uniformity (C_u) (from well-graded to uniform) but with the same mean grain size (d_{50}) (approximately equal to 1.00 mm), were tested, denoted as BS1, BS2, BS3. Blue sand has a silica content (SiO_2 > 98%), with irregularly shaped grains. A recent work by Li and Senetakis (2017) described the particle shape properties of the host soil; the sphericity (S) and roundness (R) were found to be equal to 0.54 and 0.28 respectively, based on visual observation of the grains and quantification of the particle shape descriptors adopting the empirical method proposed by Krumbein and Sloss (1963). The regularity, ρ, defined as the arithmetic mean of S and R (after Cho et al., 2006) is equal to 0.41. The specific gravity (G_s) of the blue sand is 2.65. The characteristics of the different samples used in the study are summarized in Table 1 and their grain-size distribution curves are presented in Figure 1. A representative scanning electron microscope (SEM) image of the blue sand is depicted in Figure 2. A set of thirty-three specimens from the samples denoted as BS1 to BS3, were used for model development of normalized shear modulus reduction and damping increase curves of fiber-reinforced sands, denoted as the major testing program in the study and details are given in Table 2.

A single fiber type, polypropylene fibers, denoted as PF, was used as the reinforcing material. These fibers have an average length of about 12 mm and a circular cross-section with an average diameter of 0.03 mm, and their specific gravity is equal to 0.9 (Li and Senetakis, 2017).

2.2 Materials of minor testing program

From the same host soil, two other types of sands were prepared in the laboratory named as Blue sand 4 (BS4) and Blue sand 5 (BS5) (Table 1). The sample denoted as BS4 has d_{50} =1.00 mm and C_u equal to 2.55 that was found between BS2 and BS3. The sample denoted as BS5 is relatively uniform (C_u≈1.41) but has different mean grain size in comparison to the rest samples of the study. From these two soils (BS4 and BS5), four additional specimens as well as six specimens from BS2 with different fiber contents were prepared in the laboratory and tested under high amplitude resonant column test (HARCT), named the minor testing program, for verification purposes of the developed expressions. Details of these additional ten specimens are given in Table 3. Note that samples 11 and 12 in Table 3 were not designed to verify the newly developed expressions but only to verify the effect of fiber on G_{max}, as discussed in section 3.2.

2.3 Sample preparation methods and applied stress paths

A fixed-partly fixed Hardin-type resonant column which has a system that allows the specimen to be tested in resonance while maintaining an anisotropic load up to 2 KN, was used in this study. It is only G_{vh} (waves propagating in the vertical direction with the particles vibrating in the horizontal direction) in specific that was measured in the resonant column tests to investigate the role of stress anisotropy, whereas the study of stiffness anisotropy, i.e. measurement of G_{hv} (waves propagating in the horizontal direction with the particles vibrating in the vertical direction) and G_{hh} (waves propagating in the horizontal direction with the particles vibrating in the horizontal direction) was not considered in the current work. This resonant column was recently calibrated by Li et al. (2018). The schematic sketch of the Hardin-type resonant column is shown in Figure 3, which apparatus can accommodate cylindrical specimens of 140 mm in height and 70 mm in diameter with a solid cross-section. In total, thirty-three specimens were prepared for the major testing programme based on the host sands Blue sand 1 (BS1), Blue sand 2 (BS2) and Blue sand 3 (BS3), mixed with different percentages (FC) of polypropylene fibers, equal to 0, 1 and 2% (Table 2).

Before the specimen preparation, the parent sand was first washed through the sieve No.200 (0.075mm opening size) to remove the fine-grained particles. Clean sands were then oven-dried and sieved to reach target grading characteristics. Approximately 2% to 3% of water was first added to the sand before the mixing with polypropylene fibers (a procedure that has been described by Li and Senetakis, 2017). This preparation method led to the construction of relatively uniformly distributed fibers within the soil mass. Thereafter, the moist tamping technique was used to prepare fiber reinforced specimens into a split mold of appropriate dimensions on the base pedestal of the resonant column. For unreinforced sands, the dry compaction method was used to prepare the specimens. It is noted that high amplitude resonant column tests conducted on specimens with different preparation methods (i.e. dry tamping or moist tamping) and different saturation states (i.e. dry or fully saturated) as well as different void ratios are expected to give the same stiffness degradation curves as long as pore water pressure build up is prevented during the tests on saturated specimens (Menq, 2003; Senetakis et al., 2013a; Senetakis et al., 2016). After the specimen preparation into the split mold, typical saturation processes were followed using the back-pressure technique.

The experiments were conducted at constant mean effective confining stresses (p') of 100, 300 and 500 kPa. After the first step of isotropic consolidation, the radial stress decreased and the deviatoric stress increased so that to keep a constant p' loading path. Based on this procedure, stress anisotropy effects were examined in the study (similar to Li and Senetakis, 2018b, on pure sands), but not fabric or stiffness anisotropy. At each level of (p'), high-amplitude resonant column tests (denoted as HARCT) were conducted varying the stress ratio (η=q/p') as: 0, 0.25, 0.5, 0.75 and 1. Thereafter, each given specimen at a given level of (p') was subjected to HARCT at different stress ratios. In specific, different vibration amplitudes and consequently different ranges of strain were applied on the top of the sample by increasing the amplitude of the torsional excitation. Based on this exercise, the small-strain shear modulus (G_{max}) of the specimens was quantified as well as the strain-dependent shear modulus (G) above the elastic threshold as a function of shear strain amplitude. Material damping was measured from small strains (<10^{-3}%) to medium strains (up to 10^{-1}% of shear strain) using the free vibration decay method adopting three cycles (after Stokoe et al., 1999, ASTM, 2015). The axial strains of the specimens were measured with a vertically positioned displacement transducer (LVDT), and sample volume changes were recorded directly using a volume/pressure controller. It is worth to notice that the back-pressure valve was open during the resonant column measurements to dissipate the pore water pressure. Senetakis et al. (2016) reported, based on experiments on fully saturated sands, that the pore water pressure tends to increase at medium strain resonant column excitation if the tests are conducted in an undrained state (i.e. the back-pressure valve was kept as closed in that study). Therefore, the back-pressure valve was decided to remain open during the resonant column tests to avoid pore water pressure build-up during the experiments. Details of the complete sets of experiments for the major and minor testing programs are summarized in Tables 2 and 3, respectively. Note that the same sample preparation method, test procedures and stress paths have been applied on the major and minor testing programs.

3. Results and discussion

3.1 Summary of resonant column tests of major testing program

A total number of thirty-three HARCT were conducted to develop expressions for normalized modulus reduction and damping increase curves. About twelve to thirteen resonant frequencies and damping values were recorded at a given effective pressure and stress ratio. Thus, within the set of five stress ratios (q/p') for each specimen, a total number of approximately sixty-five measurements of normalized shear modulus and sixty-five measurements of damping were collected for each specimen. The entire database of the major testing program included, approximately, 2,145 data points of shear modulus and 2,145 data points for damping, respectively. This total set of experimental data points are given in Figure 4, in terms of normalized shear modulus against shear strain amplitude and damping ratio against shear strain amplitude (termed as G/G_{max}-γ and D_s-γ curves, respectively). Upper and lower bounds of normalized stiffness reduction and damping increase curves are also plotted in Figures 4(a) and 4(b) respectively, to show some bounds of the data points herein. For simplicity, the hyperbolic model as presented by Hardin and Drnevich (1972a, 1972b) is used in Figure 4(a), which is given in Equation (1):

$$\frac{G}{G_{max}} = \frac{1}{1+\left(\frac{\gamma}{\gamma_r}\right)} \tag{1}$$

where the reference strain (γ_r) corresponded to G/G_{max} equal to 0.5 (after Darendeli, 2001, Menq, 2003). The uppermost and lowest fitting curves for G/G_{max}-γ corresponded to γ_r values equal to $1.85\times10^{-1}\%$ and $5.5\times10^{-2}\%$, respectively. The relatively wide distribution of reference strains (or, alternatively, the wide spectrum of G/G_{max} values at a given shear strain amplitude) shown in Figure 4 could be attributed to the wide spectrum of grading characteristics of the host sands, the effect of the confining stress as well as the inclusion of fibers. Li and Senetakis (2018a) have illustrated the positive contribution of fibers in terms of increase in the reference strain under isotropic loading, which, as noticed by Li and Senetakis (2018a), depends upon the grain size characteristics and type of the host sand.

In order to draw upper-lower boundary curves for damping ratio, as shown in Figure 4(b), the maximum and minimum reference strain values mentioned in Figure 4(a) were used along with the simple two-order polynomial expression proposed by

Senetakis et al. (2013a) correlating damping increase and normalized modulus reduction for sands (Equation (2)):

$$D_s - D_{s,min}(\%) = 7.22 \times \left(\frac{G}{G_{max}}\right)^2 - 25.25 \times \left(\frac{G}{G_{max}}\right) + 17.96 \tag{2}$$

In Equation (2), a small-strain damping ratio ($D_{s,min}$) of 0.50% was decided to be used for simplicity here to draw the limiting curves in Figure 4(b). In the subsequent sections, a detailed step-by-step analysis is presented in order to isolate the important factors that contribute to the wide spectrum of normalized modulus and damping values at a given strain amplitude. This analysis will implement the recent modification of the hyperbolic model of Equation (1) by Oztoprak and Bolton (2013).

3.2 Representative results under isotropic loading stress state

Typical plots of shear modulus (G)–shear strain (γ) from the HARCT for BS1 with different fiber contents at an isotropic confining pressure of 300 kPa are given in Figure 5(a), and corresponding curves normalized with a widely accepted void ratio function $f(e)= e^{-1.3}$ are given in Figure 5(b) to eliminate the effect of void ratio. It is noticed that the addition of fiber leads to a decrease of shear modulus, which is in agreement with the recent studies by Li and Senetakis (2017, 2018a). Even after decoupling the effect of void ratio, the stiffness drop is still apparent in Figure 5(b). Heineck et al. (2005) reported that the small strain shear modulus of a uniform Osorio sand reinforced with 0.5% polypropylene fibers is the same as the unreinforced specimens. However, the figure they have plotted was in logarithmic scale for both normalized effective stress and normalized G_{max} with reference pressure as 1 kPa. Therefore, the difference of G_{max} between reinforced and unreinforced specimens was minimized and G_{max} seemed to be relatively close in log-log scale. In fact, a close inspection of the data by Heineck et al. (2005) would reveal that many of the data points of the reinforced specimens were located below that of the unreinforced sand specimens, with a drop of stiffness of, approximately, 5% to 20%. Some other research works have also demonstrated the relatively unfavourable effect of fibers in term of G_{max} (i.e. small-strain stiffness drops when polypropylene fibers are added to the sand). Clariá and Vettorelo (2015) found that the presence of fibers (up to 2%) reduces the small-strain shear stiffness of the fiber reinforced soils. Michalowski and Čermák (2003) suggested that when the fiber content is greater than 0.5%, the stiffness of fiber-soil mixtures at small-strains is decreased. In addition, to directly eliminate the effect of void ratio, specimens reinforced with fibers were prepared with the same void ratio as the unreinforced one, rather than indirectly compare the normalized $G_{max}/f(e)$ values. Approximately a 30% of stiffness drop can be observed in Figure A1 between 1% fiber reinforced specimen and pure sand specimen with the same void ratio, which implies that the decrease of stiffness for the reinforced specimen is not because of the increase of void ratio. Even though there is a negative contribution of fiber content on the absolute value of shear modulus, it will be shown in the subsequent discussion that the presence of fibers leads to higher linearity of the normalized modulus reduction curves, which in turn, affects also the relationship between damping ratio and shear strain amplitude.

3.3 Representative results under anisotropic loading stress state

Figure 6 provides results of BS2 reinforced with 2% of fiber, in terms of shear modulus against shear strain at different stress ratios. These data show that the increase of stress ratio results in a greater value of shear modulus, which is in agreement with the study by Payan et al. (2016) with respect to the effect of stress ratio on the shear modulus of sands with irregular in shape grains. Gu et al. (2017) demonstrated from DEM results that the distribution of particle contact number remains nearly the same in the vertical direction under anisotropic loading, and that the soil adjusts the distribution of contact forces first to resist the external anisotropic load which leads to the increases of G_{vh}. Similarly, Jardine et al. (1999) explained that the shear wave is far more probably to travel mainly through the network of most highly stressed contacts and therefore the stiffest force chains and the strongest force chains line up with the vertical direction under anisotropic stresses, which results in the increase of shear wave velocity $V_s(vh)$ and in turn an increase of G_{vh}. In the study from Payan et al. (2016), a well-graded crushed blue sand with angular particles was found to be more sensitive to the effect of stress anisotropy in comparison with a poor-graded Sydney sand with sub-rounded particles. In the current study, the increase of shear modulus by the change of stress ratio is more pronounced for the softer fiber reinforced specimens which have lower values of shear modulus than the stiffer unreinforced specimens, which is in agreement with the study by Senetakis and Li (2017). The structure stability and non-homogeneous distribution of contact normal forces among the particles of the tested sands due to shearing might be the reason for different sensitivities of different specimens under stress anisotropy (Payan et al. 2016).

3.4Model used for the normalized modulus reduction curves fitting

Hyperbolic models first proposed by Hardin and Drnevich (1972a, 1972b) and modified by Darendelli (2001) have been widely used to describe the nonlinear soil behavior at medium strain amplitudes (e.g. Stokoe et al. 1999; Menq, 2003; Zhang et al., 2005, Senetakis et al., 2013a, 2013b; Oztoprak and Bolton, 2013; Li and Senetakis

2018a, 2018b). Recent examples of this application may refer to (Arup, 2015 and Pruiksmna, 2016). The hyperbolic model, in its latest version, proposed by Oztoprak and Bolton (2013) was adopted in the study to develop a new expression for modulus reduction curves of fiber-reinforced sands under anisotropic stress state, which is given in Equation (3):

$$\frac{G}{G_{max}} = \frac{1}{1+\left(\frac{\gamma - \gamma_e}{\gamma_r}\right)^a} \tag{3}$$

where (γ_e) is the elastic threshold taken as the strain at G/G_{max} equal to 0.99 (after Vucetic, 1994). This means that for each set of normalized modulus reduction against shear strain amplitude (i.e. given specimen at given p' and stress ratio), fitting of Equation (3) was applied and the reference strain was defined based on this fitting, whilst the elastic threshold was taken based on the experimental data or with an interpolation process. It is noticed that the expression in Equation (3) is a modified version of the hyperbolic model proposed by Darendelli (2001) on that Oztoprak and Bolton (2013) proposed, on top of the fitting parameter (a) by Darendeli (2001), an additional fitting parameter named the elastic threshold strain (γ_e) into the formula. Originally, the model was given by Hardin and Drnevich (1972a, 1972b). A discussion on the different versions of the hyperbolic model within a probabilistic framework may be found in the recent study by Akeju et al. (2019).

Figure 5(a) and Figure 6 are reproduced in Figures 7(a) and (b), respectively, by normalizing the vertical axis values with respect to the small strain shear modulus. In the data of Figure 7, fitting of the modified hyperbolic model of Equation (3) is also shown in order to draw some general view on the effect of fiber content and stress ratio on the normalized modulus reduction of the reinforced specimens. It is shown in

Figure 7(a) that the addition of fibers is effective in slightly increasing the reference strain, γ_r, ranging from 1.1×10^{-1}% for the unreinforced sand (FC=0%) to 1.3×10^{-1}% and 1.5×10^{-1}% for FC = 1% and 2%, respectively. Figure 7(b) illustrates the effect of stress ratio on the normalized modulus reduction at a given level of p'. It is shown that at a given level of the shear strain amplitude, there is a shift of G/G_{max} to greater values as the stress ratio increases.

It is noticed that once a soil is characterized in terms of its normalized modulus reduction curve and small-strain shear modulus, it is possible to reproduce the shear stress-strain curve based on the hyperbolic fitting for G/G_{max}-γ (Darendeli, 2001, Menq, 2003) as follows:

$$\tau = \mathrm{G} \times \gamma \tag{4}$$

where τ is the shear stress, G is the shear modulus ($=G_{max}\times G/G_{max}$) and γ is the shear strain. G is computed based on the measured (or modelled) G_{max} which corresponds to the small-strain shear modulus and the measured (or modelled) G/G_{max} which is the normalized modulus at respected strain amplitude. It is acknowledged that Equation (4) provides a simplified way to re-produce the stress-strain curve of a soil without accounting for post-peak softening behavior, so that its application may be restricted to methods which adopt equivalent linear response analyses, for example the codes EERA, SHAKE or QUAD4M. Figure 8 gives typical examples of the effect of the reference strain (γ_r) on the shear modulus reduction curves (Figure 8(a)) and the stress-strain curves (Figure 8(b)). It is apparent that the increase of γ_r results in an increase of the linearity of the shape of the G/G_{max}-γ curves and greater shear stresses at respected strains. It is noticed that for the example in Figure 8, the stress-strain curves are scaled to G_{max} = 300 MPa for illustration purposes.

3.5 Model parameters for normalized modulus reduction curves

3.5.1 Curvature coefficient (a)

The curvature coefficient (a), which controls the rate of the normalized modulus reduction (Darendeli, 2001), is found to decrease with the increase of stress ratio but the results exhibited some scatter. Typical plots of the fitting parameter (a) (vertical axis) against the stress ratio expressed as (q/p'+1) (horizontal axis) are shown in Figure 9 for BS3 samples reinforced with fibers. Each sub-figure corresponded to a different mean effective confining pressure and the data were fitted based on the power-law type formula of Equation (5), where k_a expresses the value of the fitting parameter (a) under an isotropic stress state and n_a expresses the rate of increase (or decrease) of (a) with the stress ratio.

$$a = k_a \times \left(\frac{q}{p'} + 1 \right)^{n_a} \tag{5}$$

As it can be seen from the results in Figure 9, which are representative of the whole database of the study, the addition of fibers seems to slow down the change of the curvature coefficient. At 300 kPa, the power n_a equalled to -0.27 for the unreinforced specimen, however, it was equal to -0.13 for BS3 with 2% fibers. Though the effect is less significant at 500 kPa in Figure 9 (b), the trend is still clear. It is concluded that the change of the curvature coefficient with stress ratio is more pronounced for unreinforced specimens than sand-fiber mixtures. From Figure 10, the curvature coefficient is relatively scattered for unreinforced sands at different confining pressures (Figure 10a), however, it is relatively close for fiber reinforced sands

(Figure 10b). It seems that fibers have minimized the effect of the effective confining pressure and the stress ratio on the curvature coefficient, homogenizing the behavior of the specimens. On the other hand, a slight increase of the curvature coefficient with the effective confining pressure was observed in Figure 10(a), which is in agreement with the findings by Menq (2003). For sands, the previous study by Oztoprak and Bolton (2013) reported on the strong dependency of the curvature coefficient on the coefficient of uniformity, however based on the data of this study, such a correlation was not clear (see Figure A2). Therefore, model parameters k_a and n_a should be correlated to fiber content and confining pressure. Figure 11 shows the three-dimensional plot of k_a – fiber content – normalized confining pressure and Figure 12 gives the correlation between the power n_a, the fiber content and the normalized confining pressure. Based on regression analysis of the results in Figures 11 and 12 using the least square method, the expressions for k_a and n_a are as follows:

$$k_a = 0.86 \times (FC + 1)^{0.04} \times \left(\frac{p'}{p_a}\right)^{0.01} \quad (6)$$

$$n_a = -0.47 \times (FC + 1)^{-0.74} \times \left(\frac{p'}{p_a}\right)^{-0.61} \quad (7)$$

Note that in Figures 11 and 12, the axis representing the fiber content is expressed as (FC+1) for convenience, so that at a zero percentage of fiber Equations (6) to (7) turn to correspond to pure sand and the similar analysis is adopted in the subsequent sections.

3.5.2 Elastic threshold strain

Oztoprak and Bolton (2013) were the first to introduce the elastic threshold strain (γ_e) to the modified hyperbolic model for better fitting purposes. γ_e is taken as the strain at

G/G_{max} equal to 0.99 (after Vucetic, 1994). A similar power-law expression was applied to γ_e in Equation (8):

$$\gamma_e = k_e \times \left(\frac{q}{p'}+1\right)^{n_e} \tag{8}$$

where γ_e is expressed as percentage (%). n_e was found to exhibit a very weak correlation with the content of fiber or the mean effective confining pressure. Within the scatter of the data, the average value of n_e was equal to -0.51 (see Figure A3). k_e was correlated reasonably well with the fiber content and the normalized confining pressure. This correlation is illustrated in Figure 13 and it is expressed analytically by Equation (9).

$$k_e = 0.001 \times \left(FC+1\right)^{0.67} \times \left(\frac{p'}{p_a}\right)^{0.22} \tag{9}$$

where γ_e in Equation (8) and k_e and FC in Equation (9) are expressed in percentage (%).

3.5.3 Reference strain

Figure 14 gives an example of representative results in terms of reference strain (vertical axis) against the stress ratio (expressed as q/p'+1) (horizontal axis) for BS1, BS2 and BS3 with a wide range of coefficients of uniformity. These data demonstrated that at a confining pressure (p') of 100 kPa, the increase of C_u leads to a more pronounced effect of the stress ratio on the reference strain. For example, for the uniformly graded sand BS3, the change of γ_r is of the order of 3.6% (increasing from 0.083% at q/p'+1=1 to 0.086% at q/p'+1=2), whereas this change is much more significant, of the order of 25% (ascending from 0.06% at at q/p'+1=1 to 0.075% at q/p'+1=2) for the well-graded sand BS1. Also, a relatively uniform soil exhibits greater linearity of the normalized modulus reduction curve in comparison to a well graded soil under isotropic loading stage at a given confining stress. These results, confirming the recent findings by Li and Senetakis (2018b) on pure sands, imply that the grading characteristics of the host soil in terms of coefficient of uniformity as well as the stress ratio play an important role on the modulus reduction curves.

In Figure 15, the effect of the stress ratio on the reference strain of specimens with different fiber contents is illustrated, considering a mean effective confining pressure of 100 kPa in Figure 15(a) and 500 kPa in Figure 15(b) and a well-graded host sand (BS1). Similar plots are given in Figures 16(a) and 16(b) for a poorly graded host sand (BS3). There is observed an apparent effect of the level of FC on the reference strain – stress ratio curve for the well-graded sand BS1 in Figure 15. At a relatively lower effective confining pressure of 100 kPa, the fitting parameter of the power law type expression (as shown in Figure 15(a)) increased from 0.06 to 0.09 with the growth of FC from 0% to 2%. Similarly, at a relatively higher effective pressure of 500 kPa, the constant fitting parameter equals to 0.11, 0.15 and 0.17 with FC = 0%,1% and 2% respectively. Similar qualitative conclusions can be drawn from the results in Figure 16. Figure 17, which shows plots of reference strain against the stress ratio for reinforced specimens of BS2, demonstrates a clear ascending relationship of the constant value with the increase in fiber content. However, the effectiveness of fiber on the power (indicating the rate of reduction of the reference strain with the increase of the stress ratio) is scattered. Note that the specimens with 0.5% and 1.5% FC in Figure 17 were only used for the verification of the developed expressions.

For the purpose of a straightforward data analysis and the development of simple but robust predictive tools, the reference strain was decided to be correlated to the stress ratio based on the following power-law expression:

$$\gamma_r = k_r \times \left(\frac{q}{p'} + 1 \right)^{n_r} \tag{10}$$

where (k_r) is a model parameter that expresses the value of the reference strain at the isotropic stress state (i.e. q/p'=0) and (n_r) is a power which expresses the sensitivity (or rate of increase) of the reference strain for increased stress ratios. Following the general trends shown in the literature, model parameter (k_r) must be related with the coefficient of uniformity and the confining pressure for granular soils. Figure 18 gives one example of this correlation in terms of a three-dimensional plot with FC=1%. Based on regression analysis using the least square method, the following expression was derived for the model parameter (k_r):

$$k_r = A \times \left(\frac{p'}{p_a} \right)^{n_1} \times \left(C_u \right)^{-n_2} \tag{11}$$

where A is a constant value, the power (n_1) expresses the sensitivity of k_r to confining pressure and the power (n_2) expresses the sensitivity of k_r to the coefficient of uniformity. As discussed in the previous section, the increase of C_u leads to a decrease of reference strain, which explains the negative sign of n_2 in Equation (11).

As can be seen in Figure 19, where A is plotted against the fiber content, a clear relationship cannot be established, so that for further analysis and model development, an average value of parameter A is used, which is equal to 0.095.

Figures 20 and 21 show the variation of the power values n_1 and n_2 against the fiber content, where the horizontal axis is expressed as (FC+1) due to the application of a power law fitting. The results show that the fitting parameter n_1 is positively affected by the fiber content, whereas the fitting parameter n_2 has a descending relationship with FC. These results imply that fiber has a homogenizing effect on the mixtures, i.e. the influence of the coefficient of uniformity becomes less important as the content of fiber increases. These observations agree qualitatively with the homogenizing influence of fiber inclusion on the static behavior of reinforced sands by Madhusudhan et al. (2017). Finally, n_1 and n_2 are expressed as a function of the content of fiber (FC) as follows:

$$n_1 = 0.32 \times \left(FC + 1\right)^{0.28} \tag{12}$$

$$n_2 = 0.23 \times \left(FC + 1\right)^{-1.25} \tag{13}$$

Similar to parameter (k_r), based on regression analysis using the least square method, the following expression was derived for the model parameter (n_r) (Figure 22):

$$n_r = 0.31 \times \left(FC + 1\right)^{0.28} \times \left(\frac{p'}{p_a}\right)^{-0.39} \tag{14}$$

3.6 Correlation between damping ratio increase and normalized stiffness reduction

For the measurement of damping ratio (D_s) in a wide range of strains, the free vibration decay method was used adopting three cycles after the cut-off of the introduced voltage to the coils (after Stokoe et al.,1999). A typical plot of the free vibration exercise on BS2 at p'=300 kPa is given in Figure 23. One simple approach in modeling damping ratio in a wide range of strains is to correlate D_s with the normalized shear modulus G/G_{max}. In this end, a second order polynomial expression is used to fit the experimental data (Equation (15)), which has been commonly used, in its general form, in the literature (e.g. Zhang et al., 2005, Senetakis et al., 2013a, 2013b). The coefficient of correlation is 0.94 for the second order polynomial expression. Alternatively, a linear expression is employed, with the coefficient of correlation to be equal to 0.93, which is shown in Equation (16). In Figure 24, the linear expression is illustrated in the fitting of damping ratio against normalized modulus reduction. Both approaches of second order polynomial and linear fitting are analytically shown in Equations (15) and (16), respectively. Note that in this analysis, damping ratio is expressed normalized as D_s-$D_{s,min}$, where $D_{s,min}$ corresponds to the small-strain damping ratio.

$$D_s - D_{s,min}(\%) = 4.2\times\left(\frac{G}{G_{max}}\right)^2 -12.8\times\left(\frac{G}{G_{max}}\right)+8.6 \qquad (15)$$

$$D_s - D_{s,min}(\%) = -6.1\times\left(\frac{G}{G_{max}}\right)+6.1 \qquad (16)$$

3.7 Comparison between measured and estimated values

Based on the modified hyperbolic model of Equation (3) and its model parameters as developed in Equations (4) -(14), Figure 25 gives a comparison between predicted and measured values of normalized shear modulus, where the measured modulus (G/G_{max}) corresponded to the major testing program (specimens No.1 to No.33 from Table 2). The difference was found to be within ±10%, which demonstrates a very good prediction of the data.

To verify the proposed new expressions, resonant column test results on three different sands with different gradations and fiber contents were considered (specimens with No.1 to No.10 in Table 3). Figure 26(a) shows that the predicted values are in excellent agreement with the measured ones (with the maximum error to be less than 10% in the majority of the data), confirming the applicability of the proposed model for the prediction of the normalized shear modulus of sands under anisotropic loading conditions. A satisfactory comparison between the measured damping ratio values from these tests and the predicted values from the new expressions can also be observed in Figure 26(b). In general, the damping values were predicted within a range of ±20%. The linear expression (Equation (16)) is used to compare measured and predicted damping ratio values in the interest of simplicity.

Based on the new expressions, design normalized modulus reduction and damping increase curves, assuming a C_u=6.0 for the host sand, at p' equal to 100 kPa and 500 kPa, stress ratios equal to 0 and 1 with 0% or 2% contents of fiber are shown in Figure 27, where in Figures 27(a) and (b) the curves are compared at an isotropic stress state and in Figures 27(c) and (d) the curves are compared at an anisotropic stress state. These curves, stemming from the data analysis and development of new expressions, highlight the important influence of fiber content (along with the important influence of the confining pressure) on the non-linear curves of fiber-reinforced sands.

4. Conclusions

The medium strain behavior of sands with different grading characteristics reinforced with polypropylene fibers subjected to stress anisotropy was studied. High-amplitude resonant column tests (HARCT) were conducted using a Hardin-type resonant column which is an effective apparatus to capture the modulus reduction and damping ratio curves of sands subjected to anisotropic stress state. Based on the study and data analysis, it was found that the addition of fibers leads to an increase of the linearity of the modulus reduction curves of the sand-fiber mixtures. It was observed that the effectiveness of fiber inclusion also depends on the grading properties of the host sand. A modified hyperbolic model was re-developed accounting for the important role of fiber content, stress ratio, coefficient of uniformity and effective confining pressure to predict normalized shear modulus for a silica sand of irregular shaped grains. For damping curves development, there was a direct correlation between damping increase and normalized modulus reduction through a linear expression. Independent experiments were conducted to verify the applicability of the newly developed expressions for polypropylene fiber-sand mixtures.

References

Akeju OV, Senetakis K, Wang Y. Bayesian parameter identification and model selection for normalized modulus reduction curves of soils. Journal of Earthquake Engineering. 2019; 23(2):305-333.

Al Refeai, T.O. Behavior of granular soils reinforced with discrete randomly oriented inclusions. Geotextiles and Geomembranes 1991;10(4):319–333.

Arup. Groningen Earthquakes Structural Upgrading Site Response Analysis; 2015. Arup report 229746_032.0_REP141, Issue Rev.0.01.

ASTM, Standard test methods for modulus and damping of soils by the resonant column method: D4015-15, Annual Book of ASTM Standards. ASTM International; 2015.

Bellotti R, Jamiolkowski M, Lo Presti DCF, O'neill DA. Anisotropy of small strain stiffness in Ticino sand. Géotechnique 1996; 46(1):115-131.

Chen G, Zhou Z, Pan H, Sun T, Li X. The influence of undrained cyclic loading patterns and consolidation states on the deformation features of saturated fine sand over a wide strain range. Engineering Geology 2016; 204: 77-93.

Cho G-C, Dodds J, Santamarina C, Particle shape on packing density, stiffness, and strength. Journal of Geotechnical and Geoenvironmental Engineering, ASCE 2006; 132(5):591-602.

Clariá JJ, Vettorelo P. Modeling of the small strain shear modulus on a fiber reinforced sand. In Proceedings of the conference of deformation characteristics of geomaterials. At Buenos Aires, Argentina. IOS Press; 2015. http://dx.doi.org/10.3233/978-1-61499-601-9-753.

Darendeli BM. Development of a new family of normalize modulus reduction and material damping curves. [Ph.D. Dissertation]. USA: University of Texas at Austin; 2001.

Diab AA, Najjar SS, Sakejk S, Taha H, Jaffal H, Alahmad M. Effect of compaction method on the undrained strength of fiber-reinforced clay. Soils and Foundations 2018;58(2):462-480.

Gu X, Hu J, Huang M. Anisotropy of elasticity and fabric of granular soils. Granular Matter 2017;19:33. https://doi.org/10.1007/s10035-017-0717-6.

Hardin BO, Drnevich VP. Shear modulus and damping in soils: Measurement and parameter effects. Journal of the Soil Mechanics and Foundations Division, ASCE 1972a; 98 (SM6):603–624.

Hardin BO, Drnevich VP. Shear modulus and damping in soils: design equations and curves. Journal of the Soil Mechanics and Foundations Division, ASCE 1972b; 98 (SM7): 667–692.

Heineck KS, Coop MR, Consoli NC. Effect of microreinforcement of soils from very small to large shear strains. Journal of Geotechnical and Geoenvironmental Engineering ASCE 2005;131(8):1024–33.

Hejazi SM, Sheikhzadeh M, Abtahi SM, Zadhoush A. A simple review of soil reinforcement by using natural and synthetic fibers. Construction and Building Materials 2012; (30): 100-116.

Ibraim E, Diambra A, Muir Wood D, Russell AR. Static liquefaction of fiber reinforced sand under monotonic loading. Geotextiles and Geomembranes 2010; 28(4): 374–385.

Ibraim E, Diambra A, Russell AR, Muir Wood D. Assessment of laboratory sample preparation for fiber reinforced sands. Geotextiles and Geomembranes 2012; 34, 69–79.

Ishihara K. Soil behavior in earthquake geotechnics, Oxford Science Publications;1996.

Jardine RJ, Kuwano R, Zdravkovic L, Thornton C. Some fundamental aspects of the pre-failure behavior of granular soils. In Proceedings of the international Symposium on Pre-failure deformation characteristics of geomaterials. 1999; 1077-1112.

Kuwado R, Connolly TM, Jardine RJ. Anisotropic Stiffness Measurements in a Stress-Path Triaxial Cell. Geotechnical Testing Journal 2000;23(2):141-157.

Krumbein WC, Sloss LL. Stratigraphy and sedimentation. 2nd ed W. H Freeman and Company; 1963.

Krishnaswamy NR, Isaac NT. Liquefaction potential of reinforced sand. Geotextiles and Geomembranes 1994;13 (1):23–41.

Kramer S L. Geotechnical earthquake engineering: Pearson Education India;1996.

Lee Junhwan, Salgado Rodrigo, Antonio J, Carraro H. Stiffness degradation and shear strength of silty sands. Can Geotech J 2004; 41: 831–843.

Li H, Senetakis K. Dynamic properties of polypropylene fiber-reinforced silica quarry sand. Soil Dynamics and Earthquake Engineering 2017;100: 224-232.

Li H, Senetakis K. Modulus reduction and damping increase of two sands reinforced with polypropylene fibers. Journal of Materials in Civil Engineering, ASCE 2018a; 30 (3):04017299.

Li H, Senetakis K. Effects of particle grading and stress state on the strain-nonlinearity of shear modulus and damping ratio of sand evaluated by resonant-column testing, Journal of Earthquake Engineering 2018b; https://doi.org/10.1080/13632469.2018.1487349 .

Li H, He H, Senetakis K. Calibration Exercise of A Hardin-Type Resonant Column. Géotechnique 2018; 68(2):171-176.

Li M, He H, Senetakis K. Behavior of carbon fiber-reinforced recycled concrete. Geosynthetics International 2017;24(5): 480-490.

Madhusudhan BN, Baudet BA, Ferreira PMV, Sammonds P. Performance of fiber reinforcement in completely decomposed granite. Journal of Geotechnical and Geoenvironmental Engineering, ASCE 2017;143(8): 04017038.

Maher MH. Gray DH. Static Response of Sands Reinforced with Randomly Distributed Fibers. Journal of Geotechnical and Geoenvironmental Engineering, ASCE 1990;116(11):1661-1677.

Maher MH, Ho YC. Mechanical properties of kaolinite/fiber soil composite. Journal of Geotechnical Engineering Division, ASCE 1994; 120 (8):1381–1393.

Maher MH, Woods HD. Dynamic response of sand reinforced with randomly distributed fibers. Journal of Geotechnical and Geoenvironmental Engineering, ASCE 1990; 116(7):1116-1131

Menq F-Y. Dynamic properties of sandy and gravelly soils. [Ph.D. dissertation]. USA: University of Texas at Austin; 2003.

Michalowski RL. Čermák J. Triaxial compression of sand reinforced with fibers. Journal of Geotechnical and Geoenvironmental Engineering, ASCE 2003;129(2):125-136.

Oztoprak S, Bolton MD. Stiffness of sands through a laboratory test database. Géotechnique 2013;63(1): 54-70.

Okur DV, Ansal A. Stiffness degradation of natural fine-grained soils during cyclic loading. Soil Dynamics and Earthquake Engineering 2007; 27: 843–854

Park T, Tan SA. Enhanced performance of reinforced soil walls by the inclusion of short fiber. Geotextiles and Geomembranes 2005;23(4):348–61.

Payan M, Khoshghalb A, Senetakis K, Khalili N. Small-strain stiffness of sand subjected to stress anisotropy, Soil Dynamics and Earthquake Engineering 2016; 88: 143-151.

Pruiksma JP. Nonlinear and equivalent linear site response analysis for the Groningen area; 2016, TNO report, TNO 2016 R10460.

Richart FE, Hall JR, Woods RD. Vibrations of soils and foundations. Prentice Hall;1970.

Senetakis K, Li H. Influence of stress anisotropy on small-strain stiffness of reinforced sand with polypropylene fibers. Soils and Foundations 2017; 57(6): 1076-1082.

Senetakis K, Anastasiadis A, Pitilakis K. Normalized shear modulus reduction and damping ratio curves of quartz sand and rhyolitic crushed rock. Soils and Foundations 2013a; 53(6): 879-893.

Senetakis K, Anastasiadis A, Pitilakis K, Coop M. The dynamics of a pumice granular soil in dry state under isotropic resonant column testing. Soil Dynamics and Earthquake Engineering 2013b; 45:70-79.

Senetakis K, Madhusudhan BN, Anastasiadis A. On the wave propagation attenuation and threshold strains of fully saturated soils with intra-particle voids. Journal of Materials in Civil Engineering ASCE 2016; 28(2): 04015108.

Stokoe K, Darendeli M, Andrus R, Brown LT. Dynamic soil properties: laboratory, field and correlation studies. In Proceedings of the 2nd international conference on earthquake geotechnical engineering. Lisbon;1999.

Tang C, Shi B, Gao W, Chen F, Cai Y. Strength and mechanical behavior of short polypropylene fiber reinforced and cement stabilized clayey soil. Geotextiles and Geomembranes 2007; 25(3): 194–202.

Tutumluer E, Kim I, Santoni L. Modulus anisotropy and shear stability of geofiber-stabilized sands. Journal of the Transportation Research Board 2004;1874:125–35.

Vucetic M. (1994). Cyclic threshold shear strains in soils. Journal of Geotechnical and Geoenvironmental Engineering, ASCE 1994;120 (12):2208–2228.

Ye B, Cheng ZR, Liu C, Zhang YD, Lu P. Liquefaction resistance of sand reinforced with randomly distributed polypropylene fibers. Geosynthetics International 2017; 24(6): 625–636.

Yetimoglu T, Salbas M. A study on the shear strength of sands reinforced with randomly distributed discrete fibers. Geotextiles and Geomembranes 2003; 21(2):103–110.

Zdravkovic L, Jardine RJ. Some anisotropic stiffness characteristics of a silt under general stress conditions. Geotechnique 47 (3): 407-437.

Zhang J, Andrus R, Juang C. Normalized shear modulus and material damping ratio relationships. Journal of Geotechnical and Geoenvironmental Engineering, ASCE 2005; 131: 453–464.

Zornberg G, Kavazanjian E. Prediction of the performance of a geogrid reinforced slope founded on solid waste. Soils and Foundations 2002;42(5):129–30.

LIST OF TABLES

Table 1. Basic Properties of tested soils

Table 2. Testing program and specimens' details for model development

Table 3. Testing program and specimens' details for model verification

LIST OF FIGURES

Figure 1. Particle size distribution curves of tested sands

Figure 2. Scanning electron microscope (SEM) images of blue sand

Figure 3. Schematic sketch of Hardin-type Resonant Column

Figure 4. Normalized shear modulus G/G_{max} (a) and damping ratio (b) against shear strain amplitude

Figure 5. Typical plots of (a) shear modulus and (b) normalized shear modulus with respect to a void ratio function against the shear strain amplitude for BS1 with 0%,1% and 2% fiber content at p'=300 kPa and $\eta+1=1$

Figure 6. Typical plots of normalized shear modulus with respect to a void ratio function against the shear strain amplitude for BS1 with 2% fiber content at p'=100 kPa and $\eta+1=1$, 1.25 and 2

Figure 7. Normalized shear modulus G/G_{max} against shear strain amplitude for (a) BS1 with 0%,1% and 2% fiber content at p'=300 kPa and $\eta+1=1$and (b) BS1 with 2% fiber content at p'=100 kPa and $\eta+1=1$, 1.25 and 2

Figure 8. (a) Normalized shear modulus against shear strain and (b) shear stress against shear strain: Ideal curves illustrating the effect of reference strain at a reference G_{max} of 300 MPa

Figure 9. Fitting parameter (a) against stress ratio for BS3 with 0%,1% and 2% fiber content at (a) p'=300 kPa and (b) p'=500 kPa

Figure 10. Fitting parameter (a) against stress ratio for (a) BS3 with 0% fiber content at p'=100,300, 500 kPa and (b) BS2 with 2% fiber content at p'=100, 300 and 500 kPa

Figure 11. Variation of k_a with normalized effective pressure and fiber content

Figure 12. Variation of n_a with the normalized effective pressure and fiber content

Figure 13. Variation of k_e with the normalized effective pressure and fiber content

Figure 14. Reference strain γ_r against stress ratio for BS1, BS2 and BS3 with 0% fiber content at p'= 100 kPa

Figure 15. Reference strain γ_r against stress ratio for BS1 with 0%,1%,2% fiber content at (a) p'=100 kPa (b) p'= 500 kPa

Figure 16. Reference strain γ_r against stress ratio for BS3 with 0%,1%,2% fiber content at (a) p'=100 kPa (b) p'= 500 kPa

Figure 17. Reference strain γ_r against stress ratio for BS2 with 0%, 0.5%,1%, 1.5% and 2% fiber content at p'= 500 kPa

Figure 18. Variation of k_r with normalized effective pressure and coefficient of uniformity at FC=1%

Figure 19. Variation of A with fiber content

Figure 20. Variation of n_1 with fiber content

Figure 21. Variation of n_2 with fiber content

Figure 22. Variation of n_r with fiber content and normalized effective pressure

Figure 23. Typical plots of free vibration decay response for BS2 at 300 kPa

Figure 24. Damping ratio against normalized shear modulus (damping is expressed as the difference between medium strain and small-strain damping)

Figure 25. Normalized shear modulus G/G_{max} predicted against measured (based on the major testing program data and the newly developed expressions)

Figure 26. Predicted against measured (a) normalized shear modulus G/G_{max} (b) damping ratio for BS2, BS4 and BS5 based on the minor testing program data and the newly developed expressions

Figure 27. Design normalized modulus reduction and damping increase curves for Cu=6, for FC=0% (host sand) and FC=2% accounting for the effect of stress ratio (Figures (a) and (b) correspond to isotropic stress state and Figures (c) and (d) correspond to q/p'=1)

Figure A1. G_{max} against normalized effective pressures for BS1 with 0% and 1% fiber content at a given void ratio

Figure A2. The variation of curvature coefficient a with Cu

Figure A3. The average value of n_e

Table 1. Basic Properties of tested soils

Sand Type	Sand Code	Grain Size Distribution		
		d_{50}(mm)	Cu	Cc*
Blue Sand 1	BS 1	0.99	5.84	1.22
Blue Sand 2	BS 2	0.96	2.98	0.88
Blue Sand 3	BS 3	1.00	1.66	0.90
Blue Sand 4	BS 4	1.00	2.55	1.02
Blue Sand 5	BS 5	1.67	1.41	0.93

*$C_C = (d_{30})^2/(d_{10} \cdot d_{60})$

Table 2. Testing program and specimens' details for model development

Sample No.	Sand type	Sample preparation method	FC (%)	Initial dry density γ_d (kN/m^3)	Initial void ratio (e)	Granular void ratio (e_{gr})	Pressure (kPa)	Stress ratio (q/p')
1	BS 1	Dry Compaction	0	16.33	0.592	0.592	100	0-1
2	BS 1	Dry Compaction	0	16.91	0.538	0.538	100	0-1
3	BS 1	Dry Compaction	0	16.74	0.553	0.553	300	0-1
4	BS 1	Dry Compaction	0	16.59	0.567	0.567	500	0-1
5	BS 1	Dry Compaction	0	16.80	0.547	0.547	500	0-1
6	BS 1	Moist Compaction	1	14.08	0.723	0.774	100	0-1
7	BS 1	Moist Compaction	1	15.80	0.615	0.662	100	0-1
8	BS 1	Moist Compaction	1	14.99	0.702	0.752	300	0-1
9	BS 1	Moist Compaction	1	14.73	0.732	0.783	500	0-1
10	BS 1	Moist Compaction	1	15.96	0.598	0.645	500	0-1
11	BS 1	Moist Compaction	2	13.45	0.861	0.971	100	0-1
12	BS 1	Moist Compaction	2	13.71	0.827	0.934	100	0-1
13	BS 1	Moist Compaction	2	14.40	0.738	0.841	300	0-1

14	BS 1	Moist Compaction	2	13.90	0.908	1.417	500	0-1
15	BS 1	Moist Compaction	2	14.47	0.731	0.833	500	0-1
16	BS 2	Dry Compaction	0	17.12	0.519	0.519	100	0-1
17	BS 2	Dry Compaction	0	16.96	0.533	0.533	300	0-1
18	BS 2	Dry Compaction	0	16.89	0.539	0.539	500	0-1
19	BS 2	Moist Compaction	1	14.70	0.735	0.787	100	0-1
20	BS 2	Moist Compaction	1	15.17	0.682	0.731	300	0-1
21	BS 2	Moist Compaction	1	14.86	0.716	0.767	500	0-1
22	BS 2	Moist Compaction	2	13.94	0.796	0.902	100	0-1
23	BS 2	Moist Compaction	2	14.08	0.779	0.883	300	0-1
24	BS 2	Moist Compaction	2	13.92	0.799	0.905	500	0-1
25	BS 3	Dry Compaction	0	15.52	0.675	0.675	100	0-1
26	BS 3	Dry Compaction	0	15.38	0.690	0.690	300	0-1
27	BS 3	Dry Compaction	0	15.45	0.682	0.682	500	0-1
28	BS 3	Moist Compaction	1	14.65	0.741	0.793	100	0-1
29	BS 3	Moist Compaction	1	14.25	0.790	0.842	300	0-1
30	BS 3	Moist Compaction	1	13.97	0.826	0.880	500	0-1
31	BS 3	Moist Compaction	2	13.09	0.913	1.025	100	0-1
32	BS 3	Moist Compaction	2	12.93	0.937	1.051	300	0-1
33	BS 3	Moist Compaction	2	13.53	0.959	1.380	500	0-1

Table 3. Testing program and specimens' details for model verification

Sample No.	Sand type	Sample preparation method	FC (%)	Initial dry density γ_d (kN/m^3)	Initial void ratio (e)	Granular void ratio (e_{gr})	Pressure (kPa)	Stress ratio (q/p')
1	BS 2	Moist Compaction	0.5	16.38	0.572	0.595	100	0-1
2	BS 2	Moist Compaction	0.5	15.98	0.611	0.635	300	0-1
3	BS 2	Moist Compaction	0.5	15.84	0.626	0.650	500	0-1
4	BS 2	Moist Compaction	1.5	15.01	0.683	0.757	100	0-1
5	BS 2	Moist Compaction	1.5	14.90	0.696	0.770	300	0-1
6	BS 2	Moist Compaction	1.5	14.80	0.708	0.783	500	0-1
7	BS 4	Moist Compaction	1	14.54	0.754	0.806	100	0-1
8	BS 4	Moist Compaction	2	13.74	0.823	0.930	300	0-1
9	BS 5	Moist Compaction	1	14.35	0.778	0.830	100	0-1
10	BS 5	Moist Compaction	2	13.74	0.823	0.930	300	0-1
11*	BS1	Dry Compaction	0	15.16	0.715	0.715	50-400	0
12*	BS1	Moist Compaction	1	14.90	0.711	0.762	50-300	0

*Additional tests to verify the negative effect of fiber on G_{max}

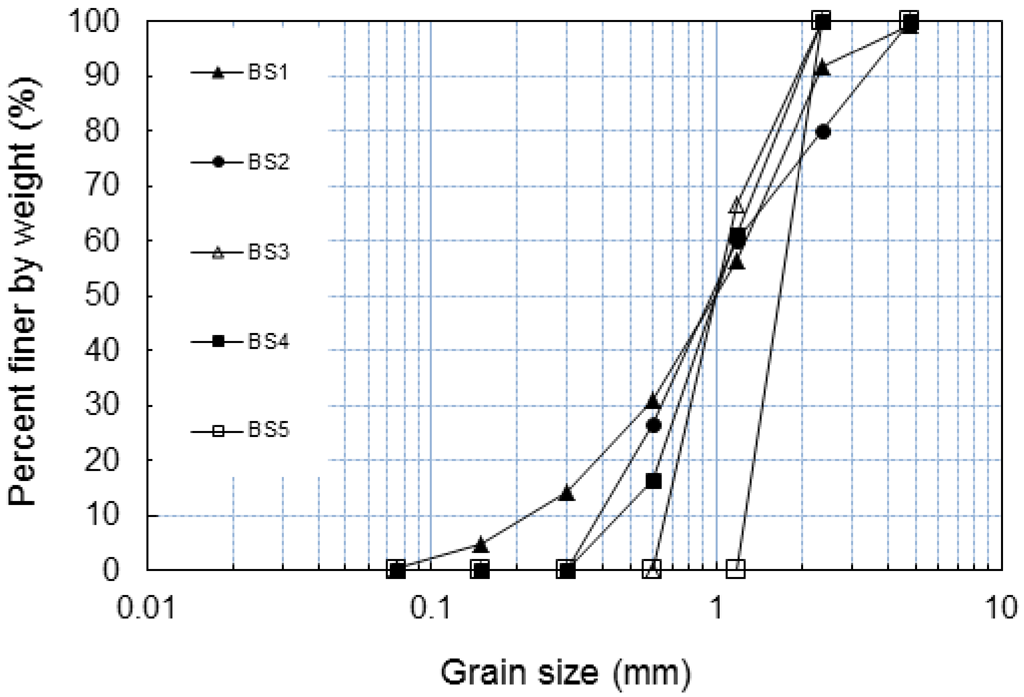

Figure 1. Particle size distribution curves of tested sands

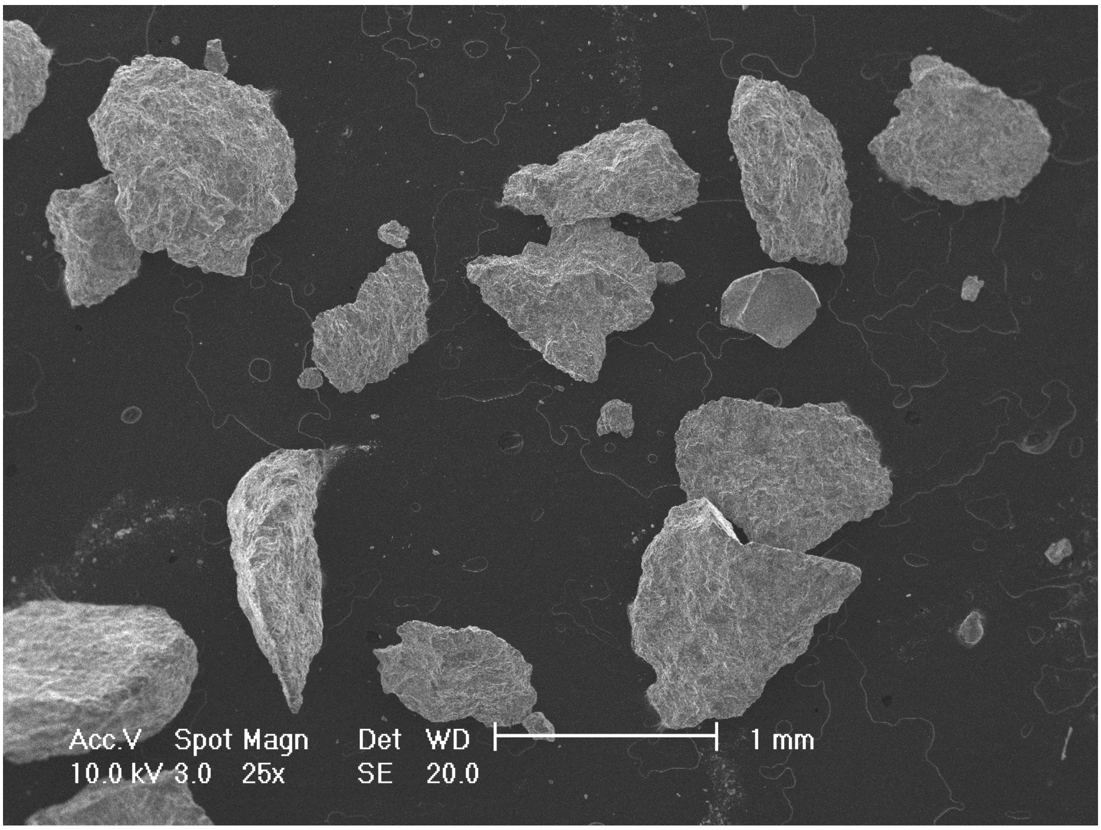

Figure 2. Scanning Electron Microscope (SEM) images of blue sand

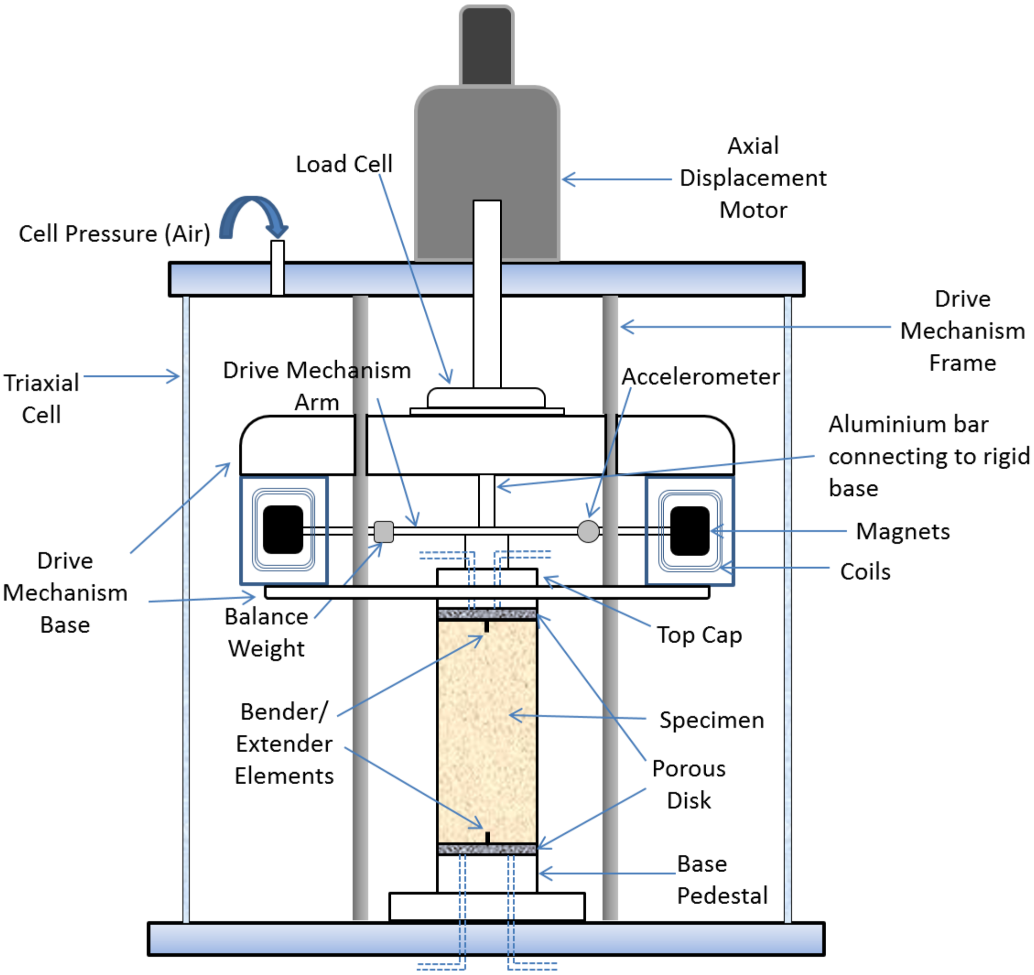

Figure 3. Schematic sketch of Hardin-type Resonant Column

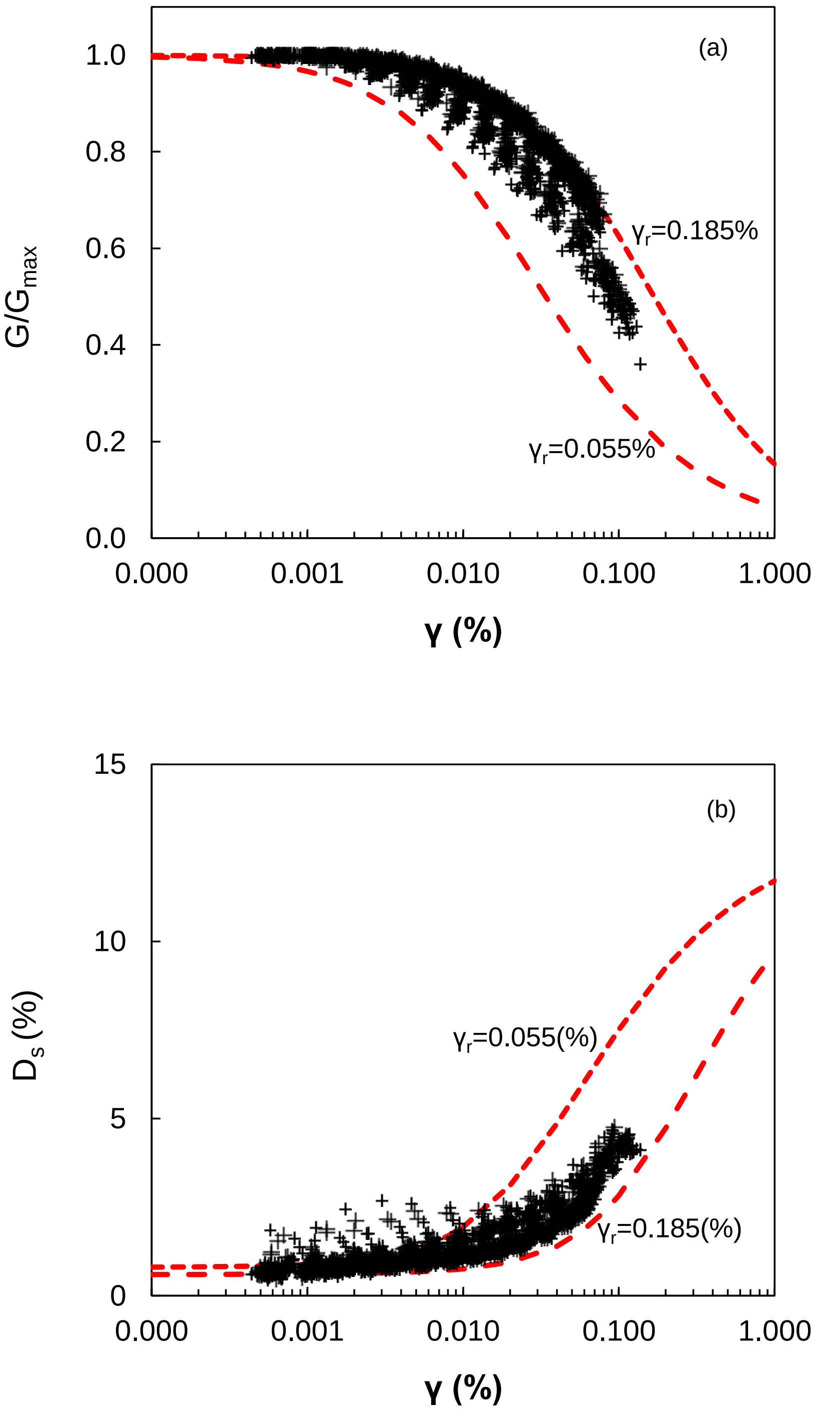

Figure 4. Normalized shear modulus G/G_{max} (a) and damping ratio (b) against shear strain amplitude

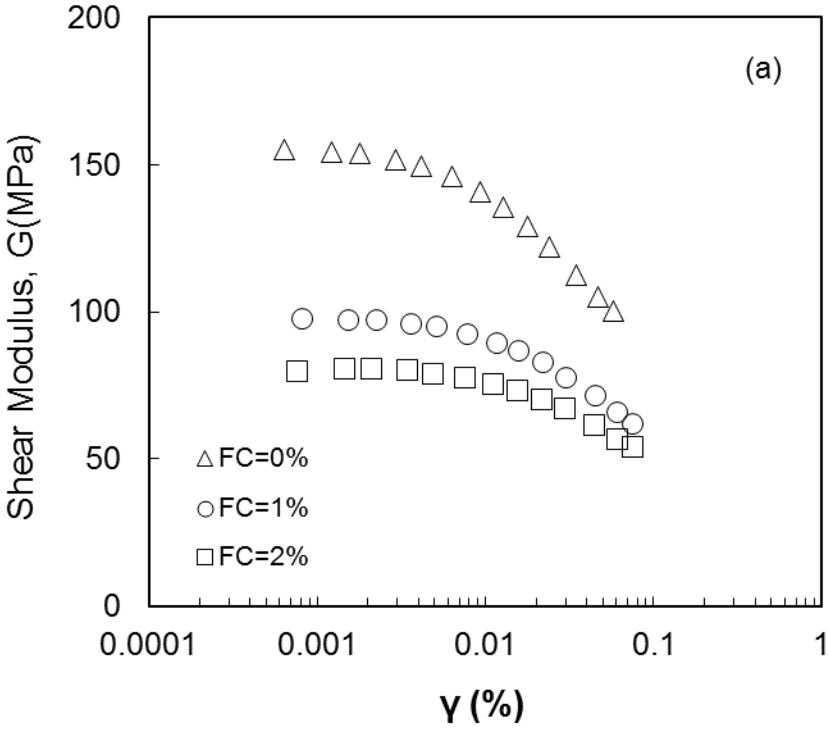

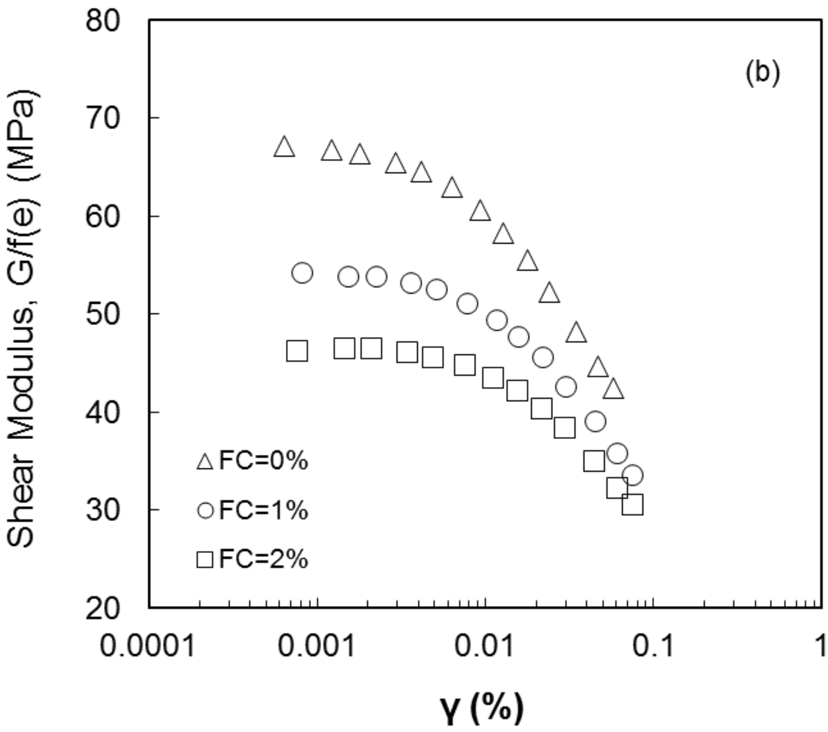

Figure 5. Typical plots of (a) shear modulus and (b) normalized shear modulus with respect to a void ratio function against the shear strain amplitude for BS1 with 0%,1% and 2% fiber content at p'=300 kPa and η+1=1

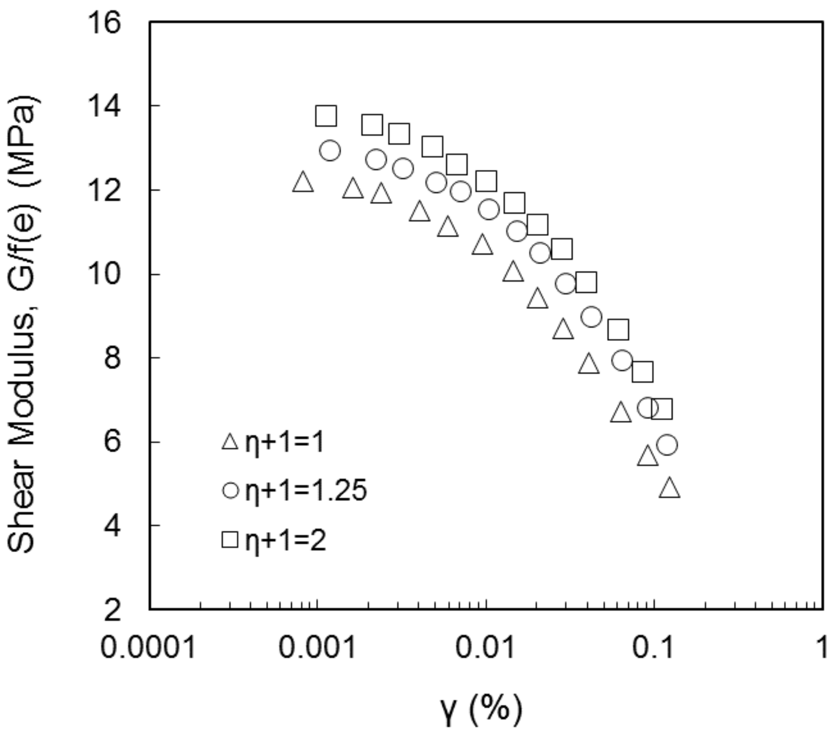

Figure 6. Typical plots of normalized shear modulus with respect to a void ratio function against the shear strain amplitude for BS1 with 2% fiber content at p'=100 kPa and η+1=1, 1.25 and 2

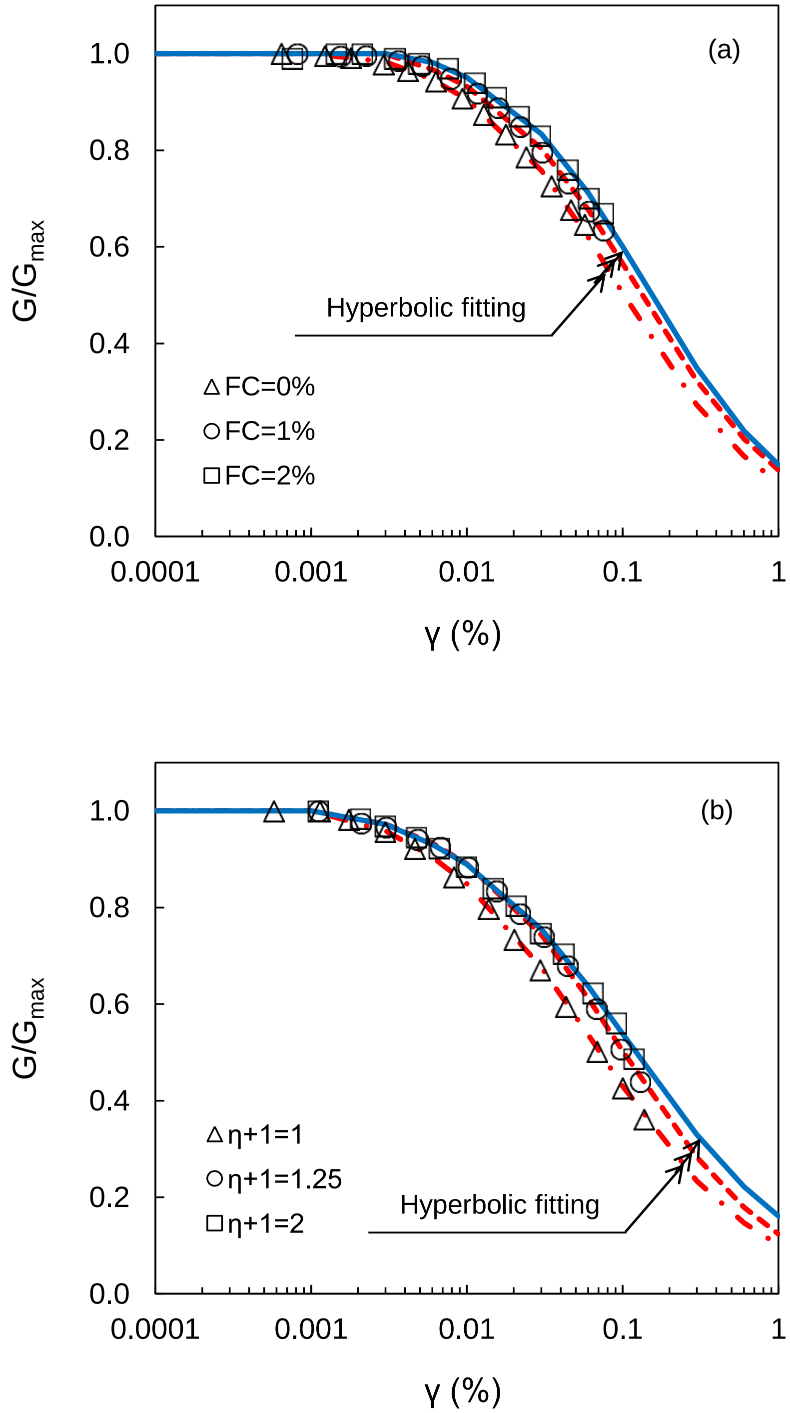

Figure 7. Normalized shear modulus G/G_{max} against shear strain amplitude for (a) BS1 with 0%,1% and 2% fiber content at p'=300 kPa and η+1=1 and (b) BS1 with 2% fiber content at p'=100 kPa and η+1=1, 1.25 and 2

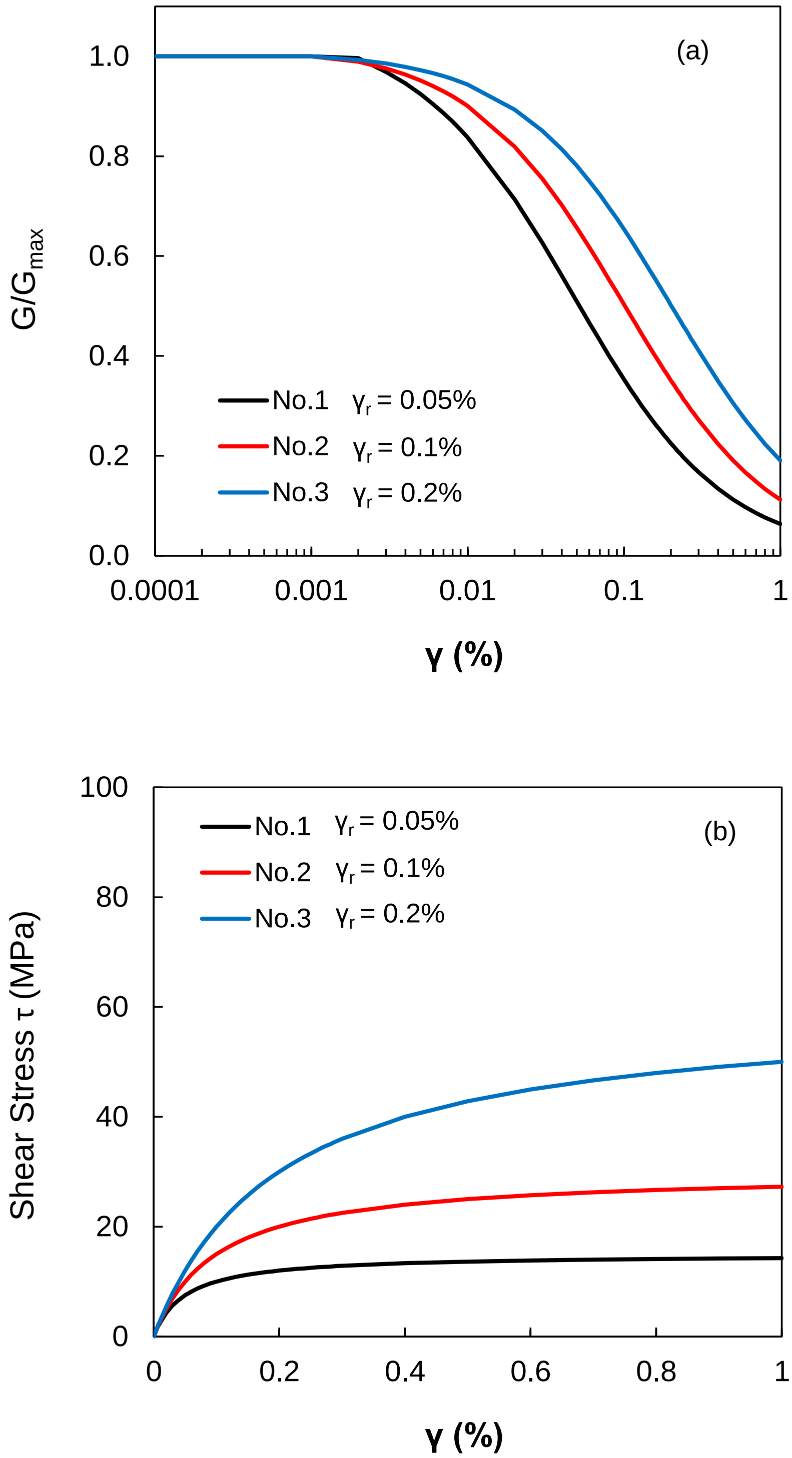

Figure 8. (a) Normalized shear modulus against shear strain and (b) shear stress against shear strain: Ideal curves illustrating the effect of reference strain at a reference G_{max} of 300 MPa

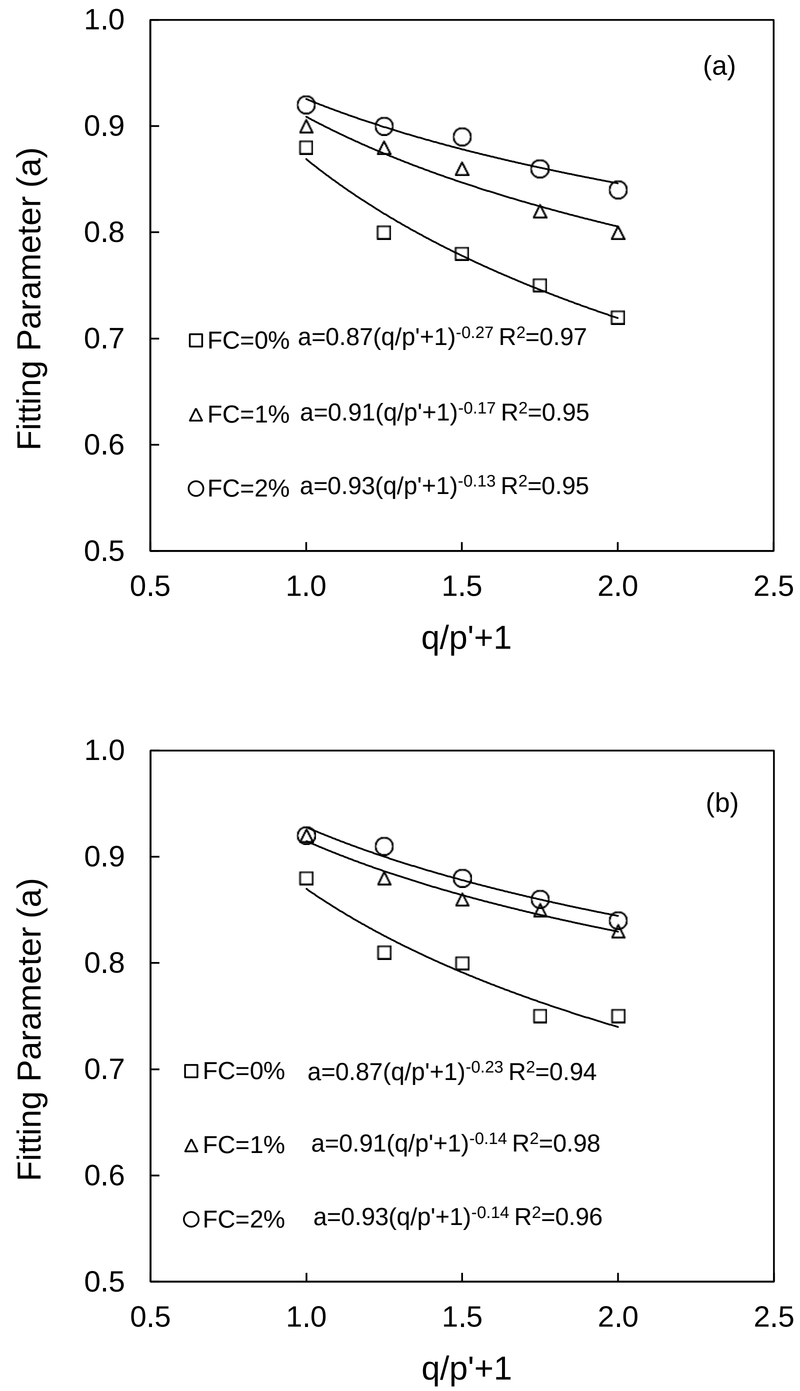

Figure 9. Fitting parameter (a) against stress ratio for BS3 with 0%,1% and 2% fiber content at (a) p'=300 kPa and (b) p'=500 kPa

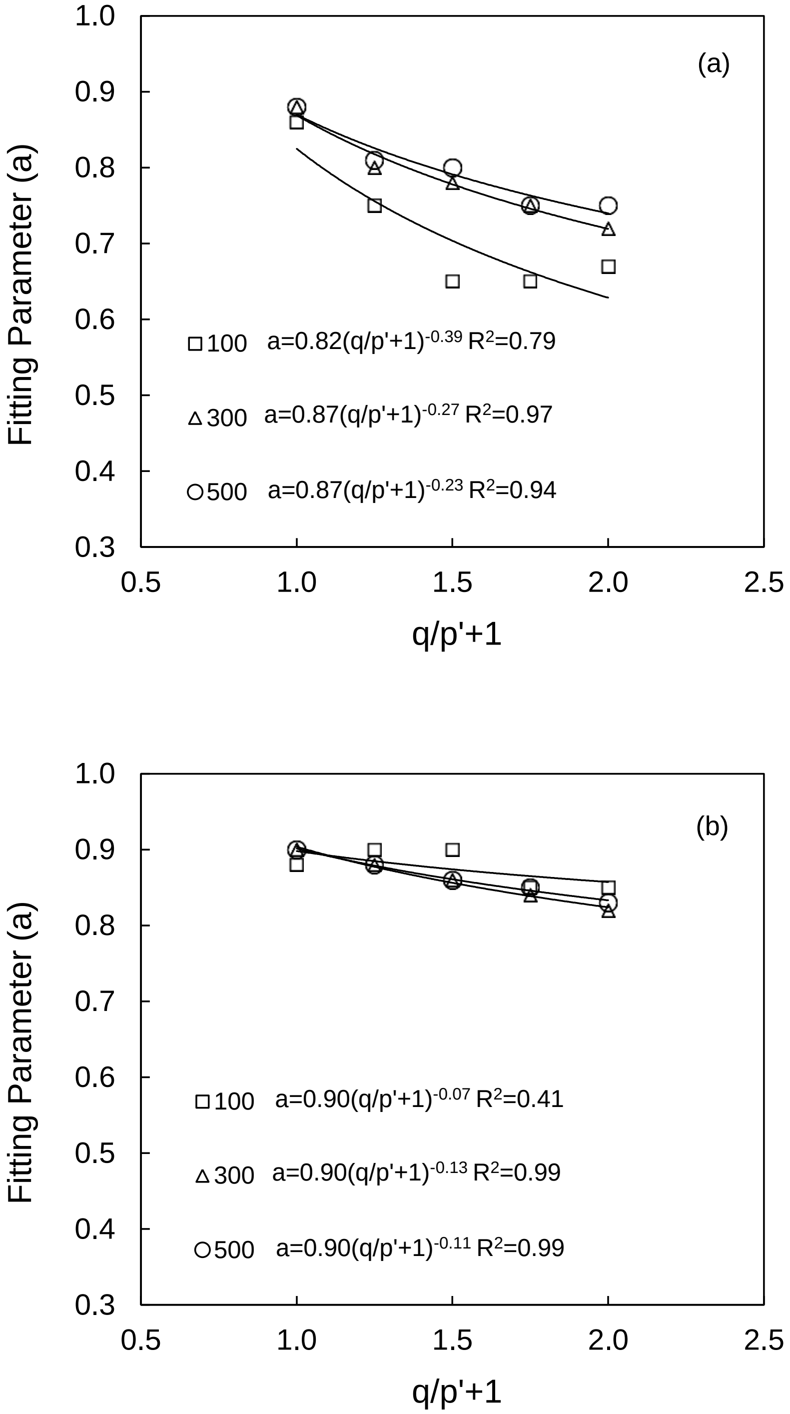

Figure 10. Fitting parameter (a) against stress ratio for (a) BS3 with 0% fiber content at p'=100,300, 500 kPa and (b) BS2 with 2% fiber content at p'=100, 300 and 500 kPa

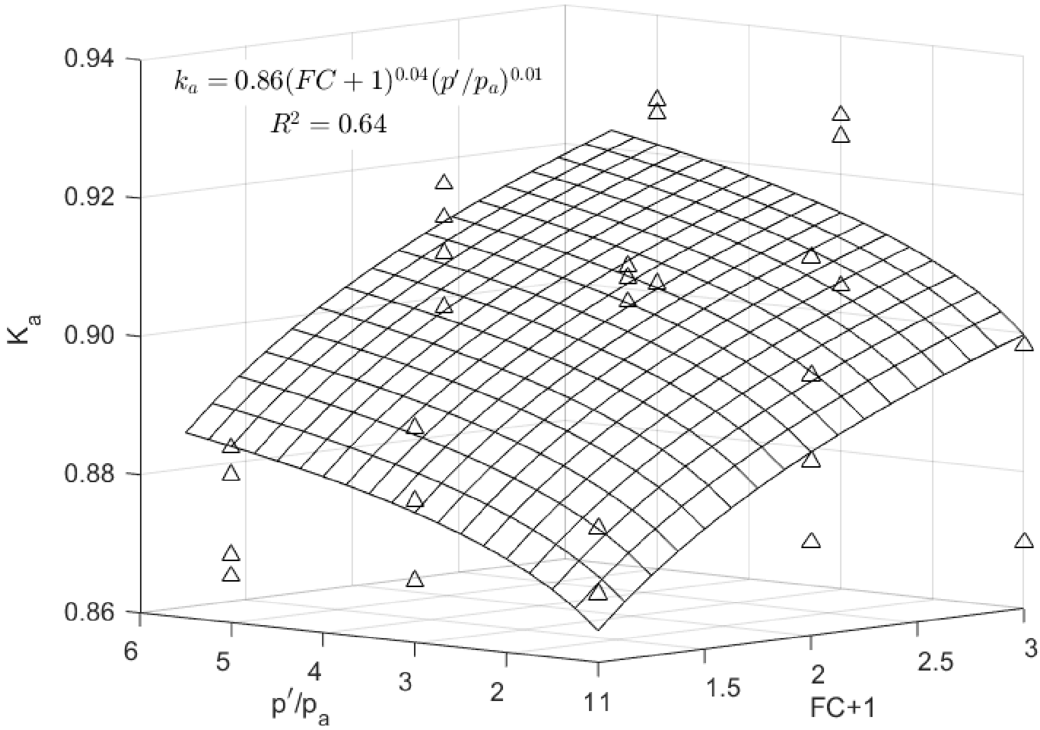

853

854 **Figure 11.** Variation of k_a with normalized effective pressure and fiber content

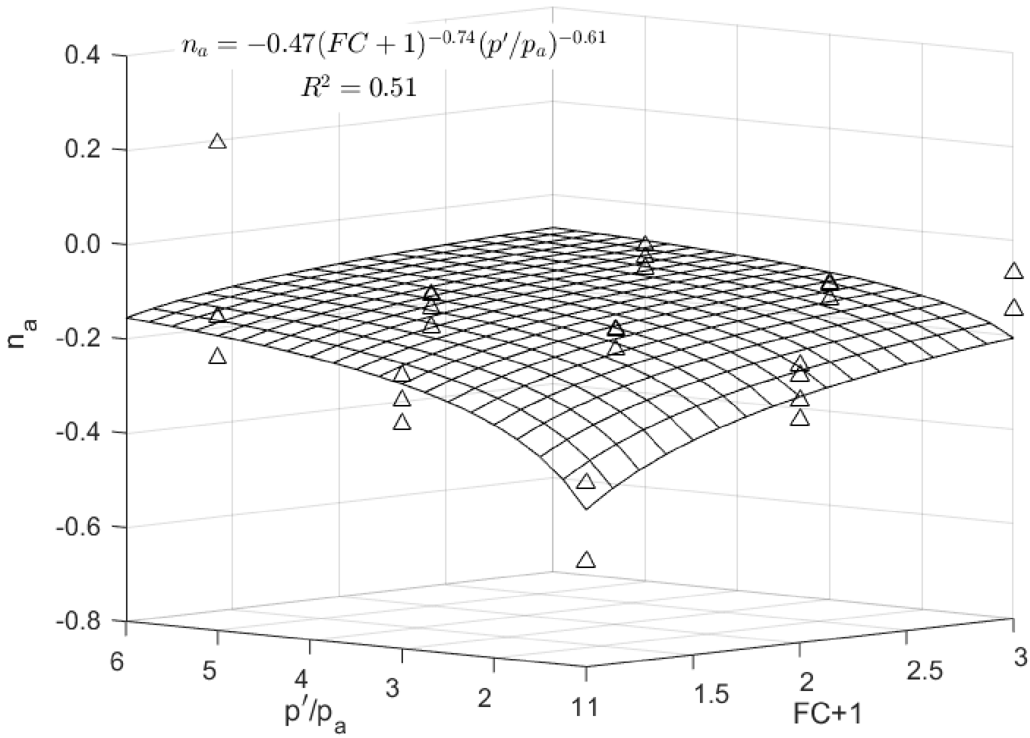

855

856 **Figure 12.** Variation of n_a with normalized effective pressure and fiber content

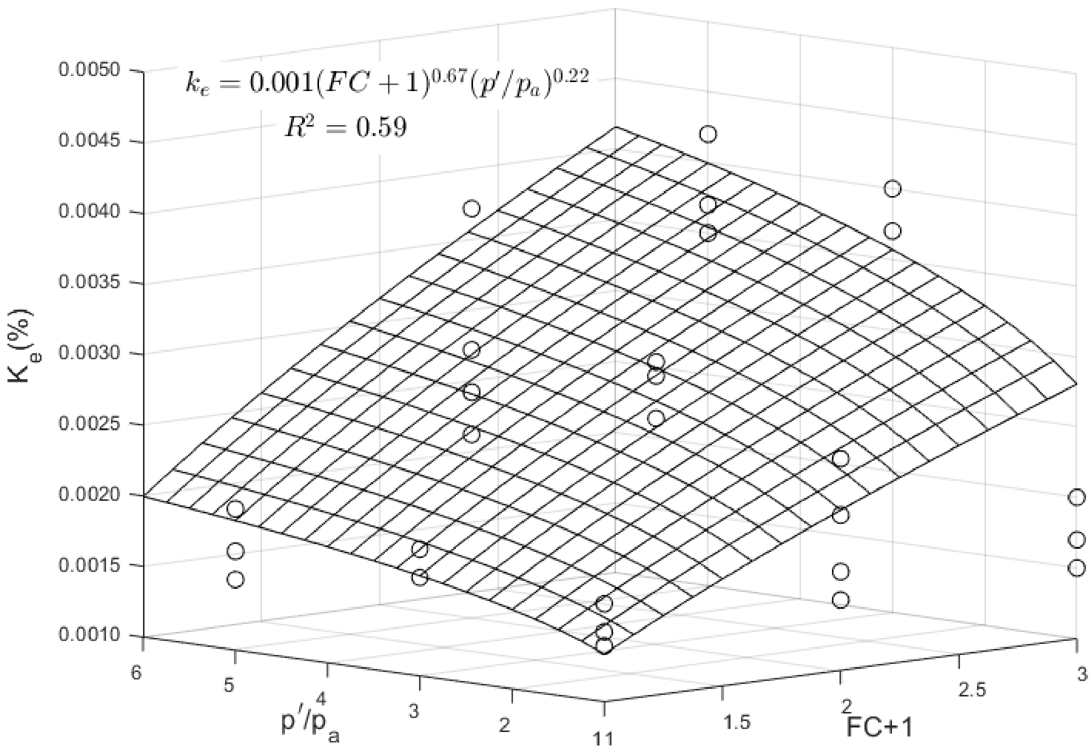

Figure 13. Variation of k_e with normalized effective pressure and fiber content

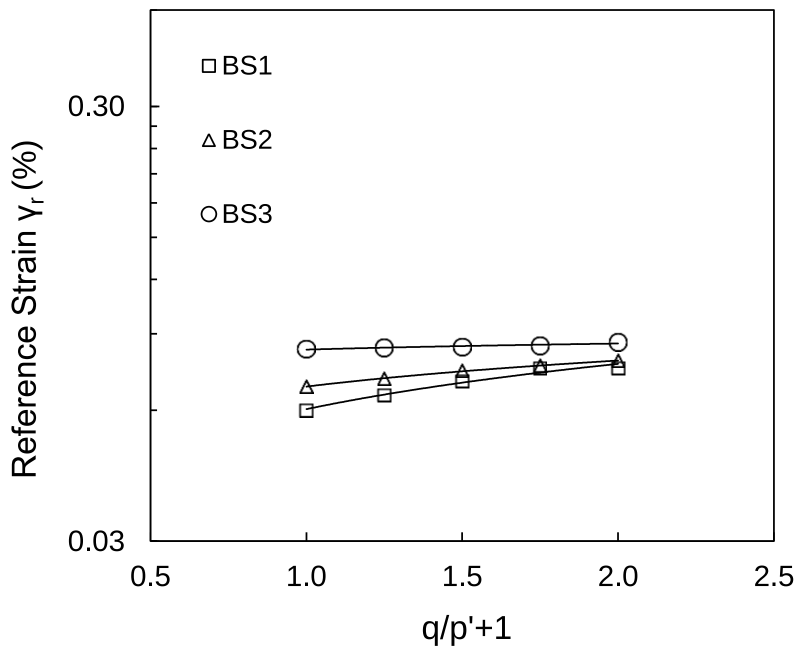

Figure 14. Reference strain γ_r against stress ratio for BS1, BS2 and BS3 with 0% fiber content at p'= 100 kPa

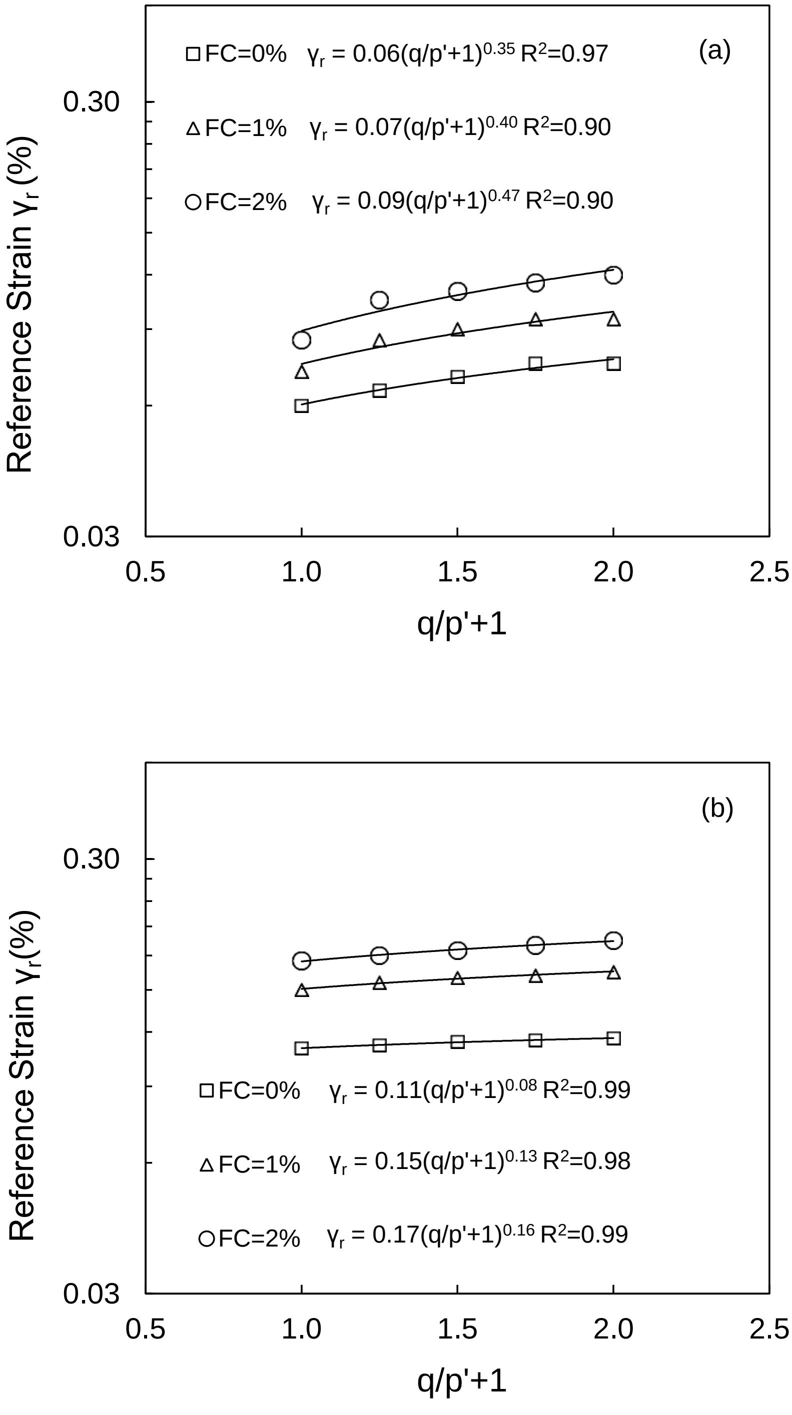

Figure 15. Reference strain γ_r against stress ratio for BS1 with 0%,1%,2% fiber content at (a) p'=100 kPa (b) p'= 500 kPa

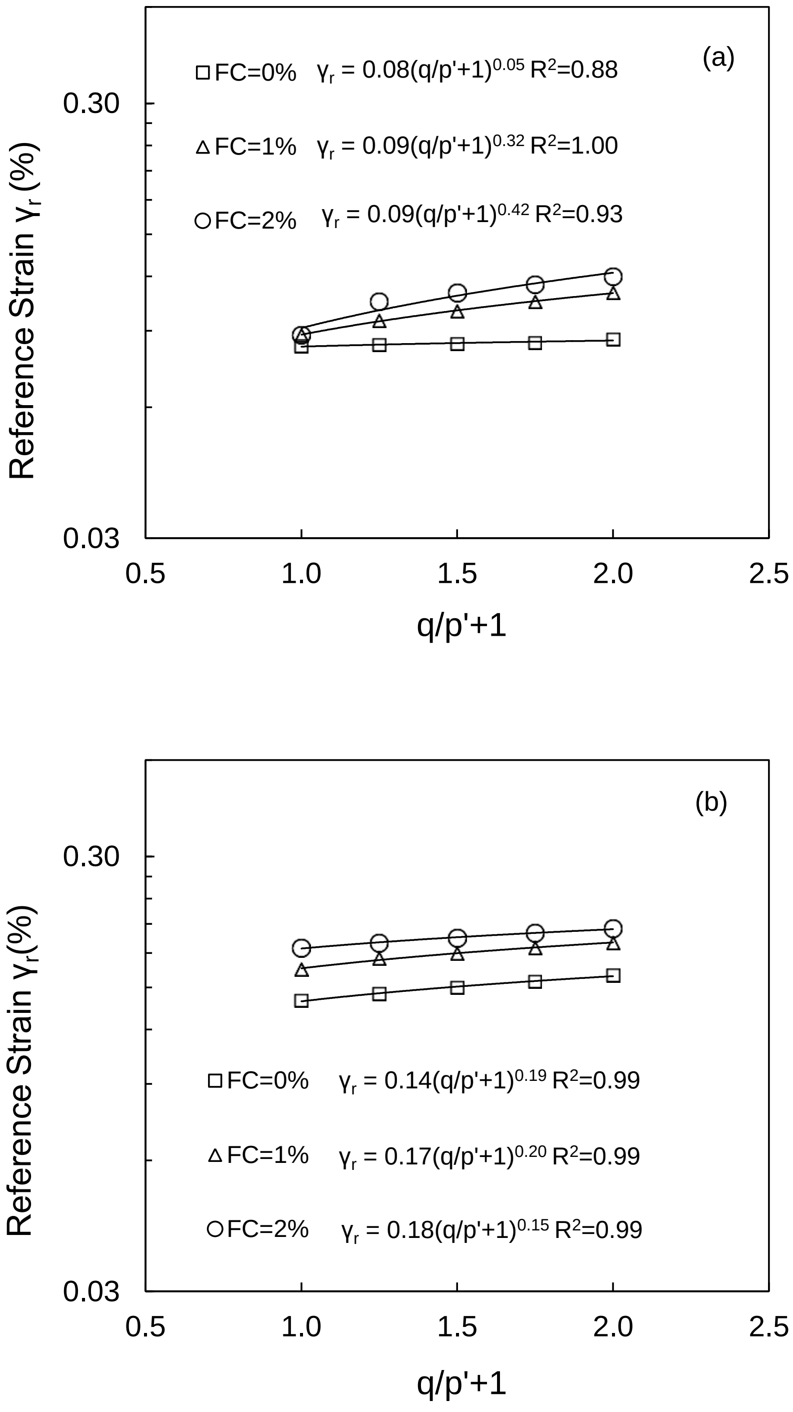

Figure 16. Reference strain γ_r against stress ratio for BS3 with 0%,1%,2% fiber content at (a) p'=100 kPa (b) p'= 500 kPa

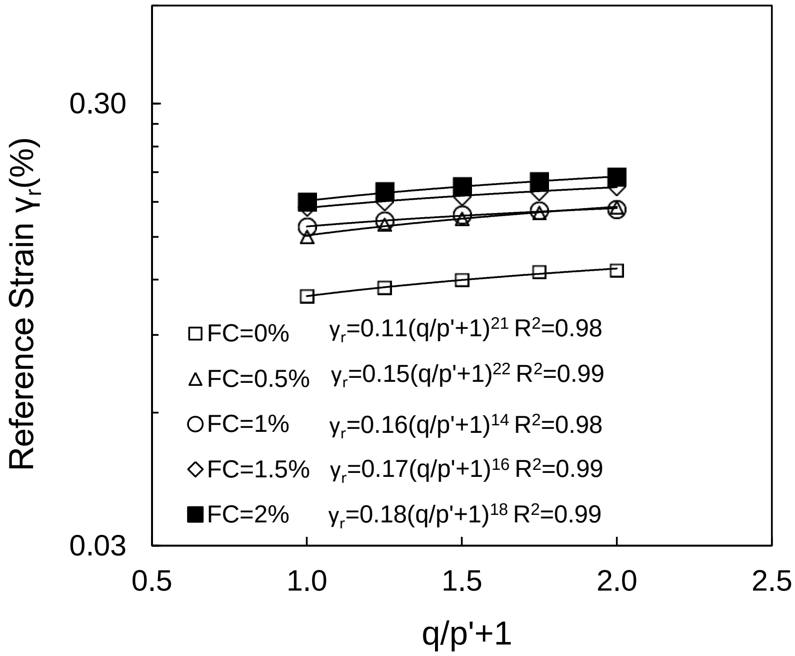

Figure 17. Reference strain γ_r against stress ratio for BS2 with 0%, 0.5%,1%, 1.5% and 2% fiber content at p'= 500 kPa

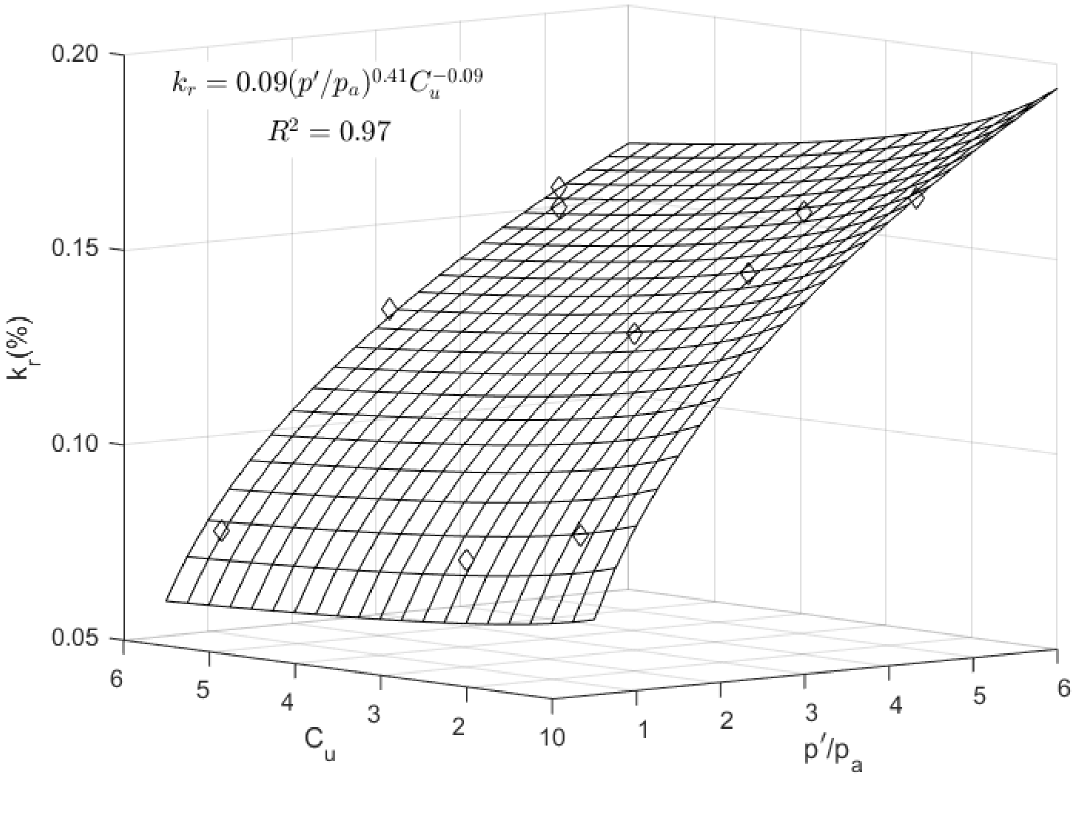

Figure 18. Variation of k_r with pressure and coefficient of uniformity at FC=1%

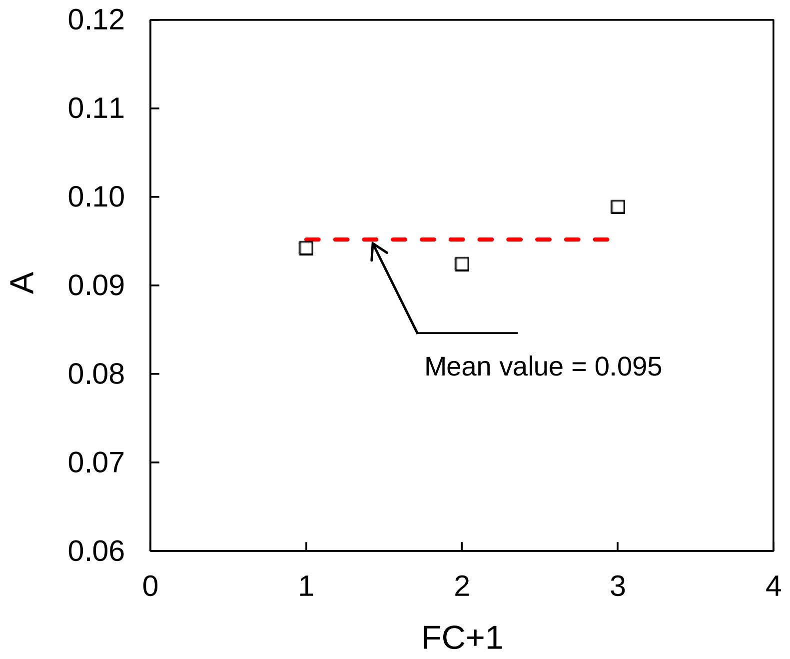

Figure 19. Variation of A with fiber content

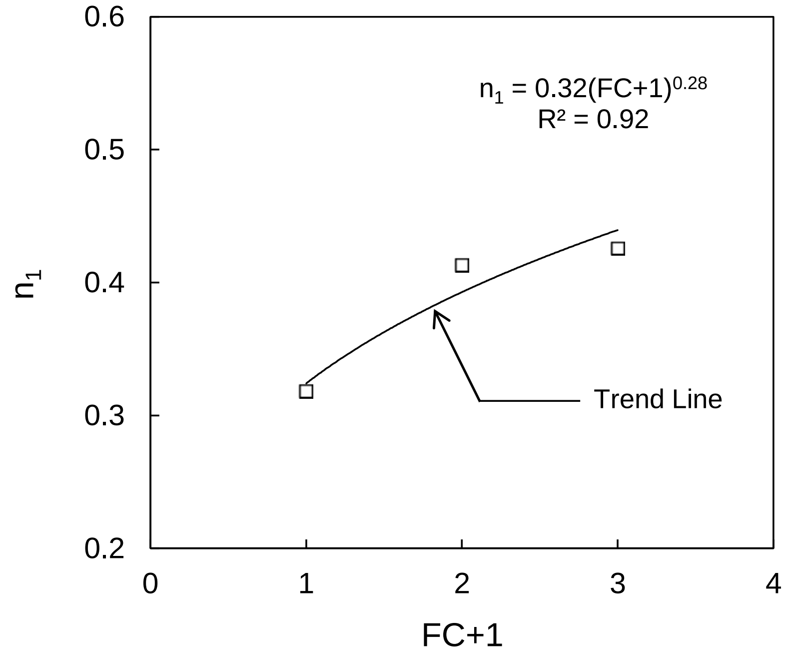

Figure 20. Variation of n_1 with fiber content

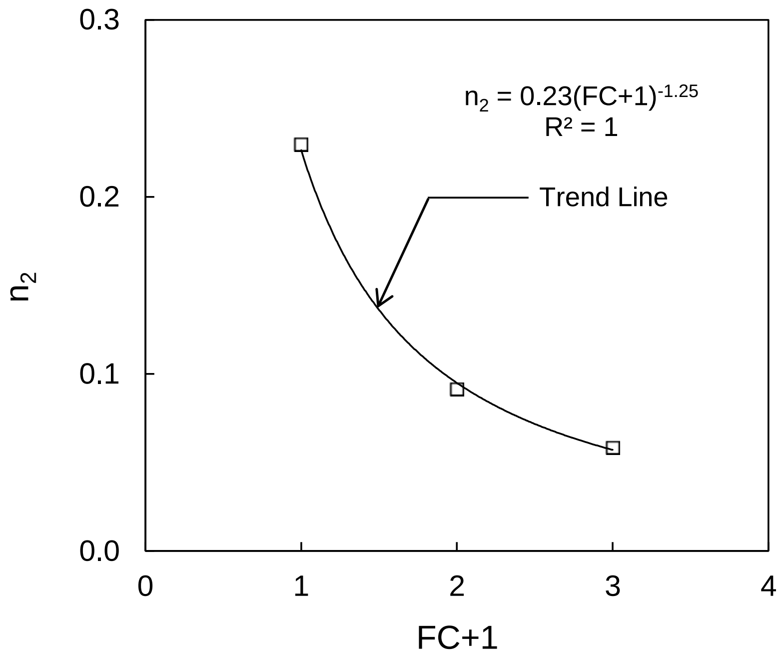

Figure 21. Variation of n_2 with fiber content

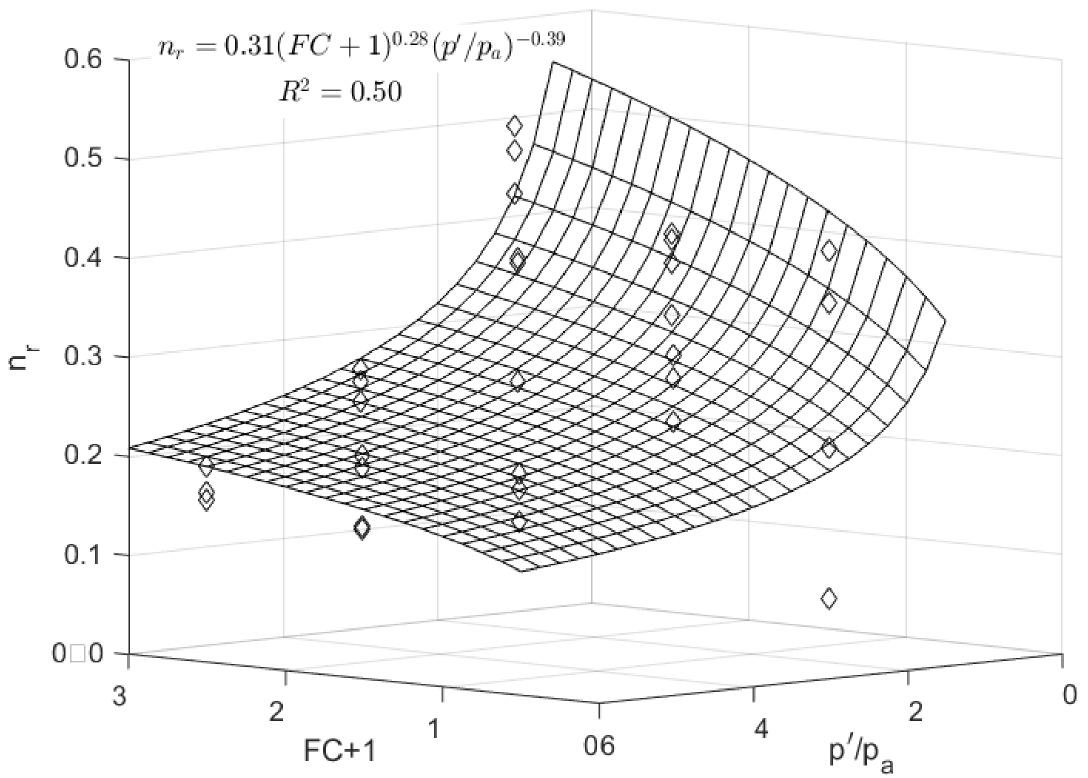

Figure 22. Variation of n_r with fiber content and normalized effective pressure

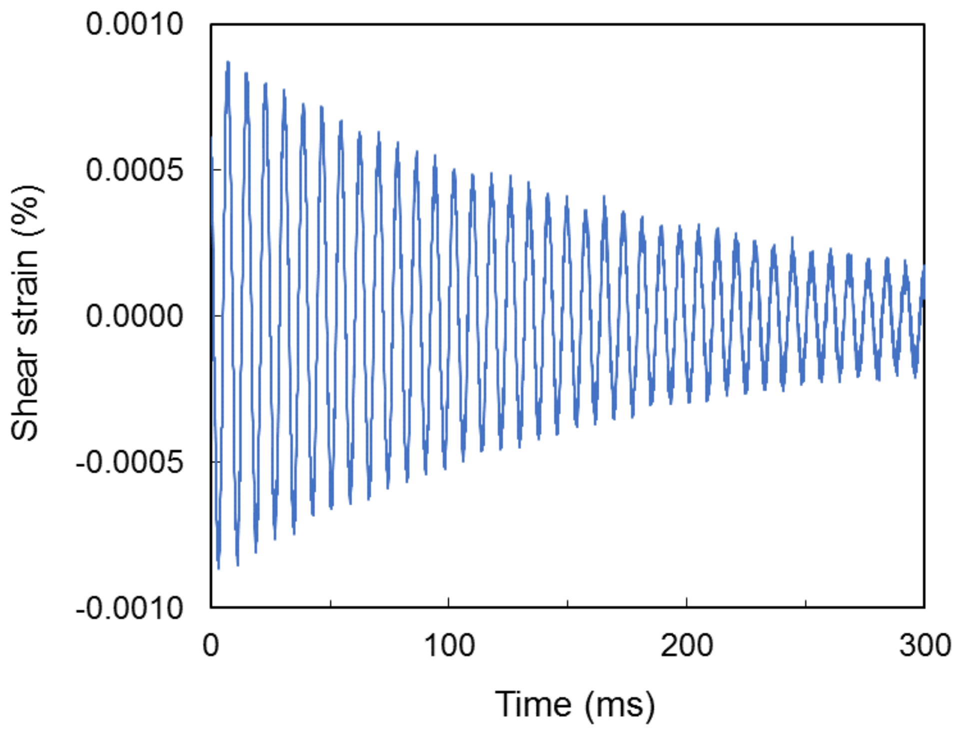

Figure 23. Typical plot of free vibration decay response for BS2 at 300 kPa

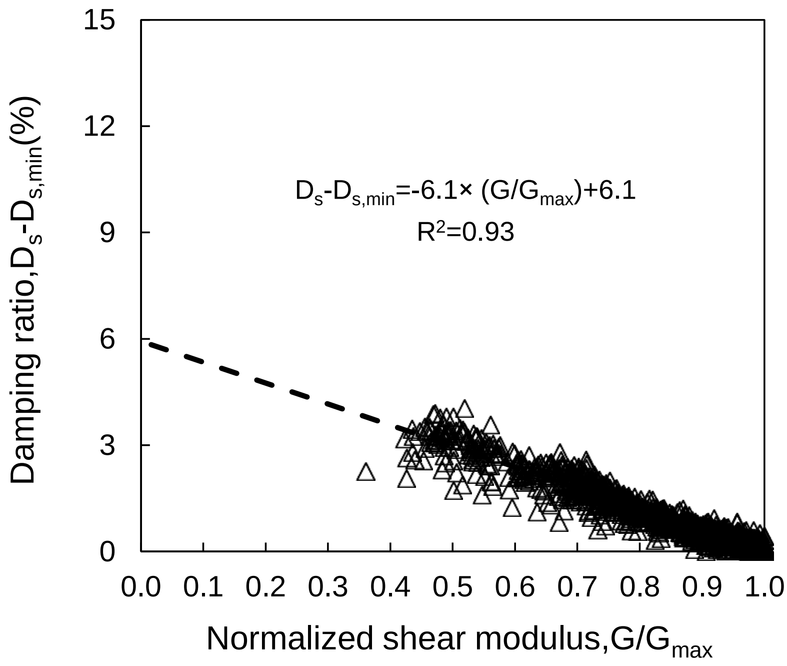

Figure 24. Damping ratio against normalized shear modulus (damping is expressed as the difference between medium strain and small-strain damping)

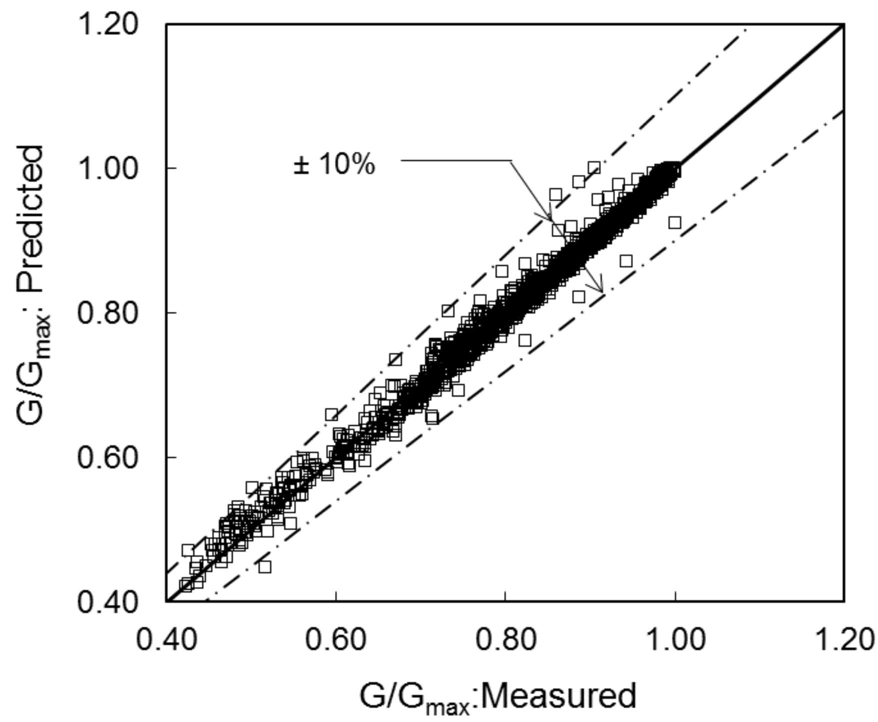

Figure 25. Normalized shear modulus G/G_{max} predicted against measured (based on the major testing program data and the newly developed expressions)

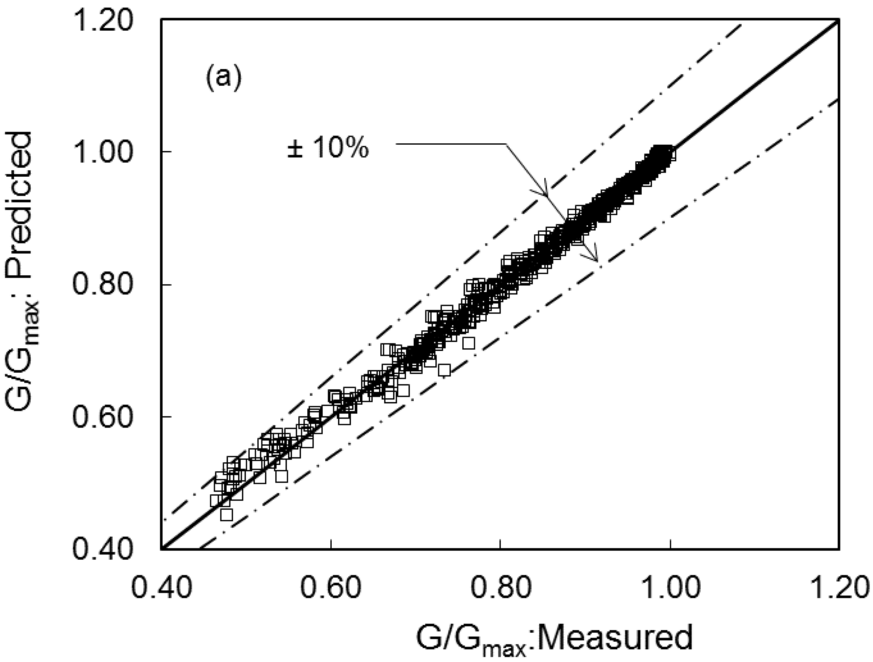

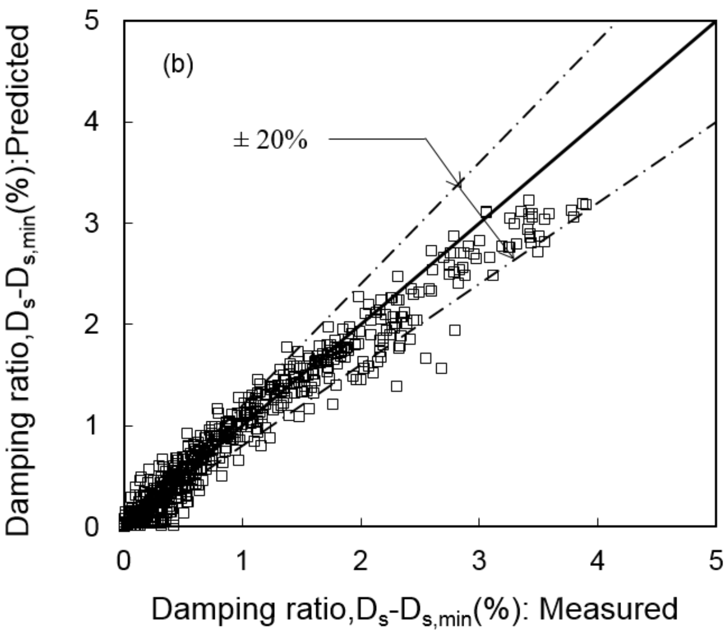

Figure 26. Predicted against measured (a) normalized shear modulus G/G_{max} (b) damping ratio for BS2, BS4 and BS5 based on the minor testing program data and the newly developed expressions

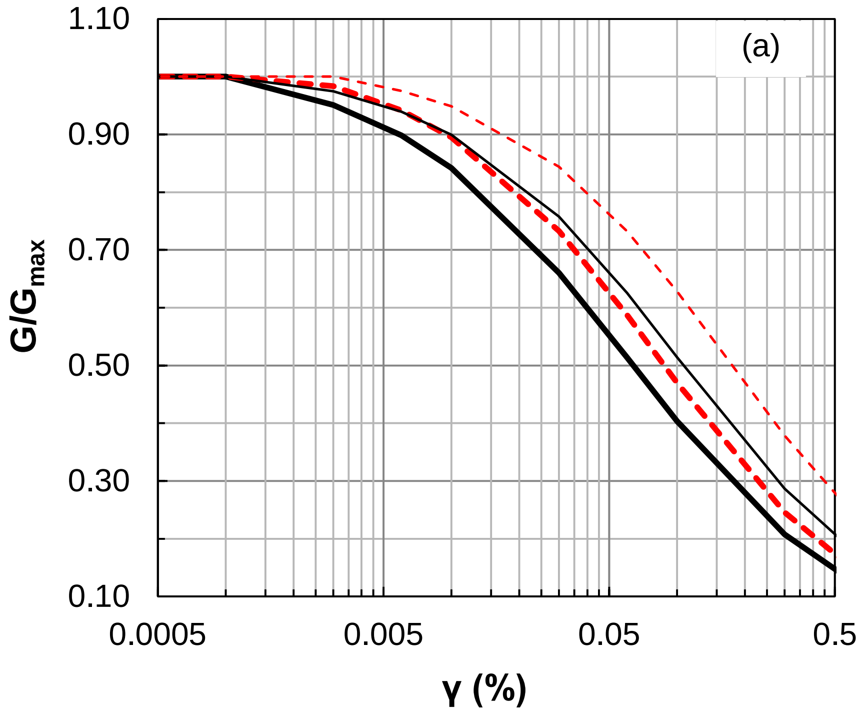
(a)
1.10
0.90
0.70
0.50
0.30
0.10
G/G$_{max}$
0.0005
0.005
0.05
0.5
γ (%)

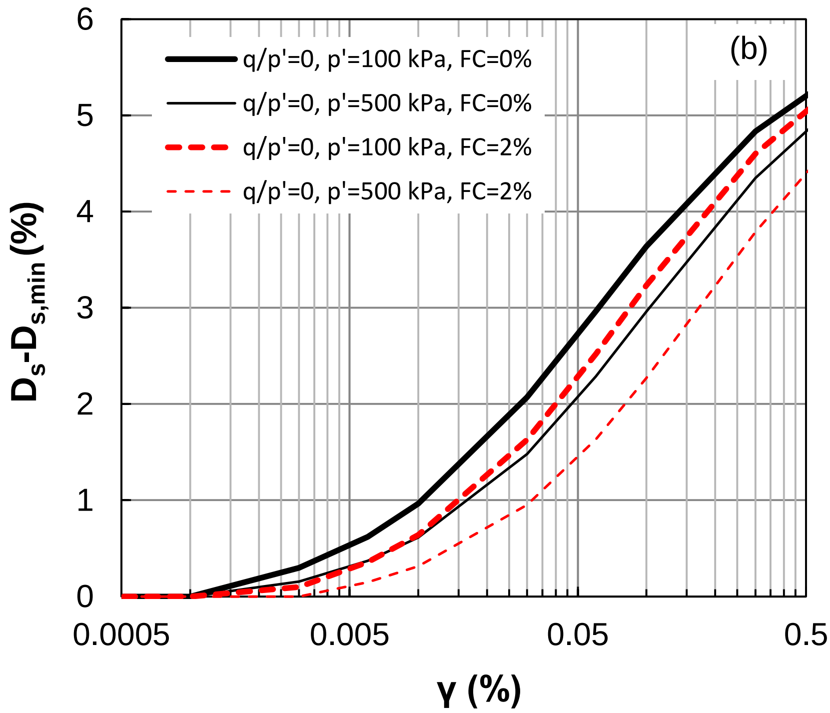
(b)
q/p'=0, p'=100 kPa, FC=0%
q/p'=0, p'=500 kPa, FC=0%
q/p'=0, p'=100 kPa, FC=2%
q/p'=0, p'=500 kPa, FC=2%
6
5
4
3
2
1
0
D$_s$-D$_{s,min}$ (%)
0.0005
0.005
0.05
0.5
γ (%)

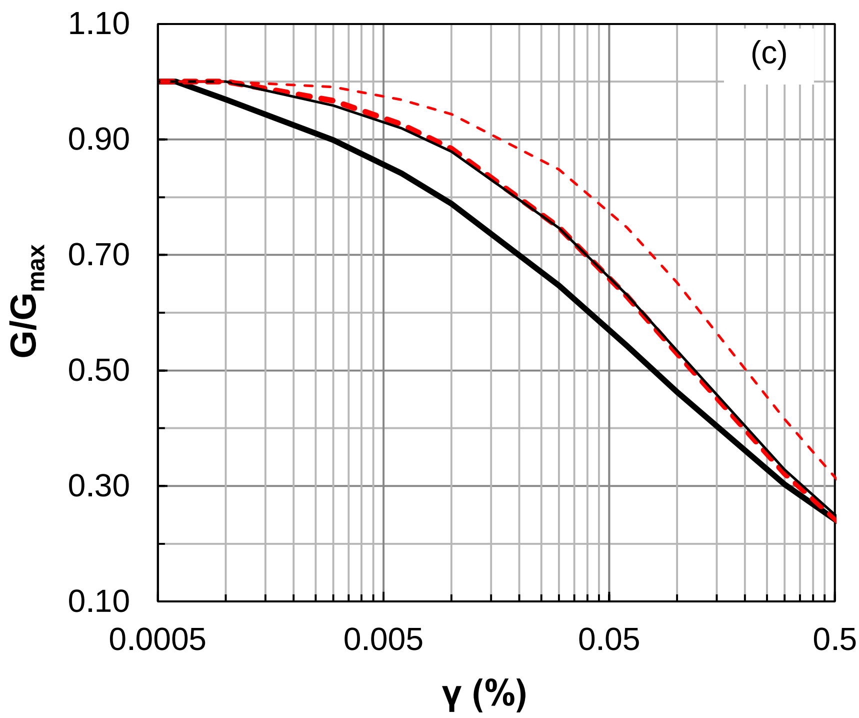

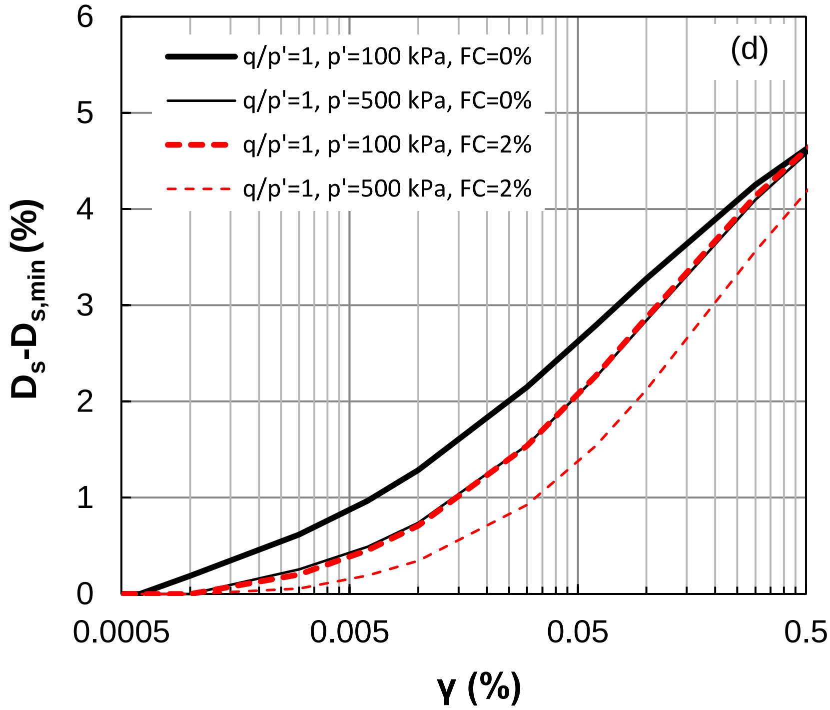

Figure 27. Design normalized modulus reduction and damping increase curves for Cu=6, for FC=0% (host sand) and FC=2% accounting for the effect of stress ratio (Figures (a) and (b) correspond to isotropic stress state and Figures (c) and (d) correspond to q/p'=1)

Appendix A

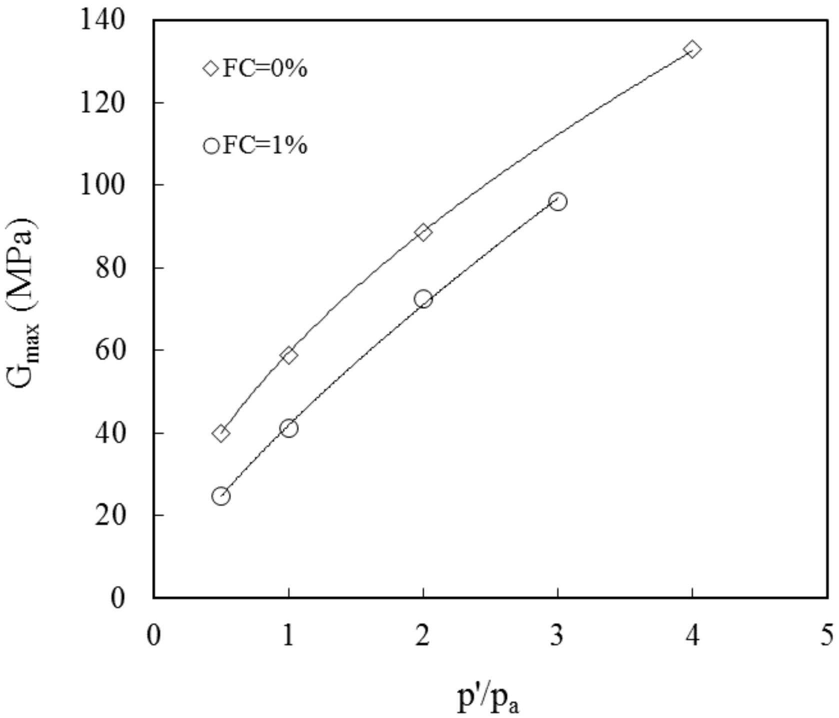

Figure A1. G_{max} against normalized effective pressures for BS1 with 0% and 1% fiber content at a given void ratio

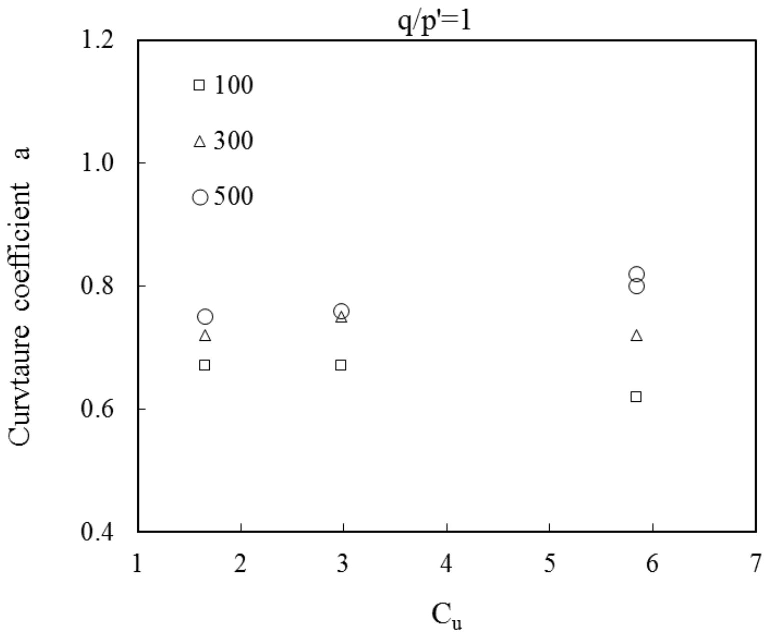

Figure A2. The variation of curvature coefficient a with C_u

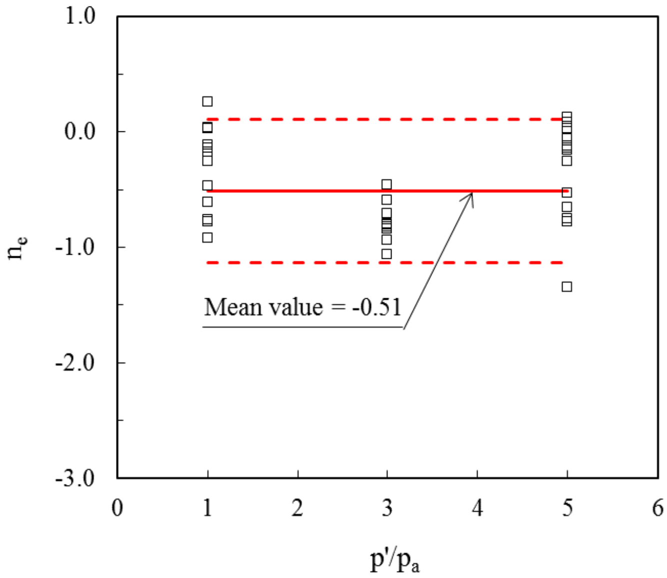

Figure A3. The average value of n_e